DOI:
10.1080/17435390.2017.1342011

Document Version
Peer reviewed version

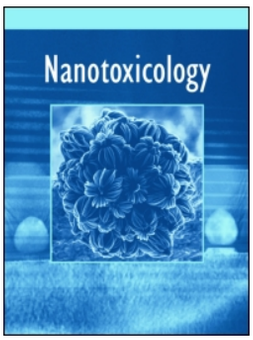

Nanotoxicology

ISSN: 1743-5390 (Print) 1743-5404 (Online) Journal homepage: http://www.tandfonline.com/loi/inan20

Toxicogenomics of iron oxide nanoparticles in the nematode C. elegans

Laura Gonzalez-Moragas, Si-Ming Yu, Núria Benseny-Cases, Stephen Stürzenbaum, Anna Roig & Anna Laromaine

To cite this article: Laura Gonzalez-Moragas, Si-Ming Yu, Núria Benseny-Cases, Stephen Stürzenbaum, Anna Roig & Anna Laromaine (2017): Toxicogenomics of iron oxide nanoparticles in the nematode C. elegans, Nanotoxicology, DOI: 10.1080/17435390.2017.1342011

To link to this article: http://dx.doi.org/10.1080/17435390.2017.1342011

Accepted author version posted online: 15 Jun 2017.

Toxicogenomics of iron oxide nanoparticles in the nematode *C. elegans*

Laura Gonzalez-Moragas[1], Si-Ming Yu[1,2], Núria Benseny-Cases[3], Stephen Stürzenbaum*[4], Anna Roig*[1], Anna Laromaine*[1]

1 Institut de Ciència de Materials de Barcelona, ICMAB-CSIC. Campus UAB. 08193 Bellaterra, Barcelona - Spain.

2 Key Laboratory of Biomaterials of Guangdong Higher Education Institutes, Department of Biomedical Engineering, Jinan University, Guangzhou 510632, China.

3 ALBA Synchrotron Light Source, Carrer de la Llum 2−26, 08290 Cerdanyola del Vallès, Barcelona, Spain.

4 King's College London. Faculty of Life Sciences & Medicine, Analytical and Environmental Sciences Division, 150 Stamford Street, London SE1 9NH - United Kingdom.

Corresponding authors:

Stephen Stürzenbaum: stephen.sturzenbaum@kcl.ac.uk

Anna Roig: roig@icmab.es

Anna Laromaine: alaromaine@icmab.es

Toxicogenomics of iron oxide nanoparticles in the nematode *C. elegans*

We present a mechanistic study of the effect of iron oxide nanoparticles (SPIONs) in *C. elegans* combining a genome-wide analysis with the investigation of specific molecular markers frequently linked to nanotoxicity. The effects of two different coatings were explored: citrate, an anionic stabilizer, and bovine serum albumin, as a pre-formed protein corona. The transcriptomic study identified differentially expressed genes following an exposure to SPIONs. The expression of genes involved in oxidative stress, metal detoxification response, endocytosis, intestinal integrity and iron homeostasis was quantitatively evaluated. The role of oxidative stress was confirmed by gene expression analysis and by synchrotron Fourier Transform infrared microscopy based on the higher tissue oxidation of NP-treated animals. The observed transcriptional modulation of key signaling pathways such as MAPK and Wnt suggests that SPIONs might be endocytosed by clathrin-mediated processes, a putative mechanism of nanotoxicity which deserves further mechanistic investigations.

Keywords: Toxicogenomics, nanotoxicity, *C. elegans*, iron oxide nanoparticles, protein corona.

Introduction

The unique properties of nanomaterials offer promising avenues in medicine; however they also raise concerns about their safety. The toxicological profiles of a wide range of nanomaterials have been determined using different *in vitro* and *in vivo* models, several exposure modes and entrance routes.(Krug, 2014) Nanotoxic effects reported vary among cell lines, organisms and/or the nanoparticle (NP) type, which can be mostly attributed to the multidimensional response mechanisms due to the physicochemical properties of the nanomaterial.(Soenen *et al.*, 2011)

Transcriptomic studies can help to elucidate the molecular mechanisms involved in NP response and pinpoint key genes able to predict the toxicity or the genetic susceptibility to different NP properties.(Nuwaysir *et al.*, 1999, Aardema and MacGregor, 2002, Poma and Di Giorgio, 2008) This research field, coined nanotoxicogenomics, will further our understanding on nanotoxicity mechanisms.(Tino *et al.*, 2014) High-throughput approaches like microarrays or next generation sequencing can be combined with 'gene by gene' techniques, mainly qPCR, which are highly quantitative and sensitive to interrogate a relatively small number of transcripts in a larger set of samples.(Pareek *et al.*, 2011) Therefore, transcriptome analysis can identify pathways and specific transcripts that are affected by NP treatment and may act as relevant molecular markers. However, these mechanistic cues should be confirmed by post-hoc

histological analysis or specific genetic experiments to test the importance and significance of the pathways identified.(Poma and Di Giorgio, 2008, Elingarami *et al.*, 2013, Tino *et al.*, 2014)

Nanotoxicogenomic studies can be performed in nanoparticle-treated cells, simple invertebrates(Poynton *et al.*, 2012, Starnes *et al.*, 2016) or more complex vertebrates (Truong *et al.*, 2013, Teeguarden *et al.*, 2014). Invertebrate models share many biological traits with vertebrates, yet offer a simpler platform to conduct mechanistic experiments in a time and cost efficient manner complying with the ethical principles known as 3Rs.(Ohno, 2002, Lehner, 2013) *Caenorhabditis elegans* (*C. elegans*) has attracted considerable attention as a model organism to evaluate inorganic nanoparticles.(Zhao *et al.*, 2013, Gonzalez-Moragas *et al.*, 2015a) Several toxicogenomic studies have provided evidence that titanium oxide, gold and silver nanoparticles induce nanotoxic mechanisms in *C. elegans.*(Tsyusko *et al.*, 2012, Rocheleau *et al.*, 2015, Starnes *et al.*, 2016) However, further research on different NP composition, sizes and surface properties is required to correlate the physicochemical properties of the materials with the molecular effects. Starnes *et al*. examined the toxicogenomic responses of pristine Ag-NP, sulfidized Ag-NPs, and $AgNO_3$ in *C. elegans*. The authors exposed the nematodes at the EC30 (effect concentration 30%) for reproduction and reported 571 differentially expressed genes, of which only 11% were common to all three treatments. Ag-NPs mainly targeted processes related to metabolism, while the suldifized Ag-NP were linked to processes related to molting and the cuticle. In the case of $AgNO_3$, the most affected processes were related stress. Rocheleau *et al*. investigated the toxicity of anatase and rutile NPs (two different TiO_2 crystallographic phases) and bulk TiO_2 particles in *C. elegans*. Whole-genome microarrays revealed that the regulation of glutathione-S-transferase (*gst-3*), cytochrome P450 (*cypp33-c11*), stress resistance regulator (*scl-1*), oxidoreductase (*wah-1*) and embryonic development (*pod-2*) genes were significantly modulated by both bulk and nano-sized TiO_2. Moreover, the authors observed a phase-dependency: anatase NPs exerted a greater effect on metabolic pathways, while rutile NPs impaired developmental processes to a greater extent. The toxicogenomic study performed by Tsyusko *et al.* revealed that 4-nm citrate-coated Au-NPs resulted in a differential expression of 797 genes at the LC_{10} (lethal concentration 10%) level. The authors identified several biological pathways associated with these genes, among them unfolded protein response and endoplasmic reticulum stress. The authors also evaluated the response of endocytosis mutants (*chc-1* and *rme-2*) to Au-NPs, concluding that the endocytosis pathway was induced by Au-NPs. This highlights that the toxicogenomic efforts combined with follow-up studies involving genetic, biochemical and imaging tools are required to confirm the mechanistic clues identified in whole-genome experiments.

In this work, we exposed the model organism *C. elegans* to iron oxide nanoparticle to study the molecular pathways affected by NP exposure. In particular, we treated *C. elegans* with 6-nm superparamagnetic iron oxide nanoparticles (SPIONs) coated with citrate and albumin to delineate differences in the transcriptome that are dependent on the chemistry of the NP coating. We interrogated the whole transcriptome of *C. elegans* by microarray analysis and performed single-gene studies by qPCR to validate the toxicogenomic experiments and to generate a hypothetical model driving the toxicity of SPIONs. We also investigated the role of oxidative stress by synchrotron Fourier Transform infrared microscopy (SR-μFTIR) to quantify lipid oxidation, as part of our proposed model.

Methods

Materials

Caenorhabditis elegans Bristol strain N2 and *Escherichia coli* OP50 were obtained from the *Caenorhabditis* Genetic Center (CGC). Peptone, yeast extract, bacteriological agar and tryptone were purchased from Conda Lab. All other reagents were bought from Sigma-Aldrich, if not stated otherwise.

Synthesis of SPIONs

A microwave-assisted route was used to synthesize Cit-SPION, as described previously.(Yu *et al.*, 2014) Briefly, 0.35 mmol iron acetylacetonate were dissolved in 4.5 mL benzyl alcohol in a microwave glass tube and vortexed for 30 seconds. Reaction tubes were transferred to the microwave reactor and the following heating ramp was applied: 1) 5 min at 60 ºC, 2) 10 min reaction at 180 ºC, 3) cooling down to 50 ºC using compressed nitrogen. After the reaction, 150 µL of 10 wt.% trisodium citrate was added and SPIONs were three times with acetone. Finally, the Cit-SPION pellet was dried at 60 ºC and redispersed in Milli-Q H_2O.

We adsorbed a monolayer of BSA onto the Cit-SPIONs as previously described.(Yu *et al.*, 2014) Briefly, 1.6 ml of a dispersion containing 1 mg/mL Cit-SPIONs was prepared using Milli-Q H_2O, the pH was adjusted to 11 by adding 0.1 M NaOH and then 200 µl of 25 mg/mL BSA solution was added. The tube was vortexed for 5 min and after 1 hour, the pH was adjusted to 7.4 by adding 0.06 M HNO_3. To remove excess of BSA, the dispersion was centrifuged using centrifugal concentrators of 100 000 MWCO (Vivaspin 6, Sartorius) for 30 min at 3000 rpm three times. Finally, BSA-SPIONs were resuspended to 2 ml using Milli-Q water.

Synthesis of Au-NPs

The 11-nm citrate-coated gold nanoparticles (Au-NPs) were synthesized by the Frens Turkevich synthesis, as described previously.(Turkevich *et al.*, 1951, Frens, 1973) Briefly, a solution of 2 mL of trisodium citrate (38.8 mM) was added to 20 ml of gold chloride

($HAuCl_4 \cdot 3H_2O$, 1 mM) at 100 ^oC under stirring. The solution was kept at 100 ^oC for 10 min or until it turned deep red.

NP Characterization

NP concentration was determined by flame absorption spectroscopy (air-acetylene) with a Perkin-Elmer 2100 spectrometer. Briefly, NP dispersions were sonicated 10 min in an ultrasound bath, diluted with HCl (1%), and the resulting solution was analyzed using a Perkin-Elmer 2100 spectrometer.

All NPs were characterized by TEM, DLS, and zeta potential. Transmission electron microscopy (TEM) samples were prepared by placing one drop of the corresponding NP dispersion on the copper grid, blotting the copper grid with a filter paper, and allowing a complete evaporation at room temperature. In the case of BSA-SPIONs, an additional step of negative staining was applied to stain protein in white; 5 µL of 2% uranyl acetate were placed on the grid for 1 min before draining off. TEM samples were imaged with a JEOL JEM-1210 electron microscope at an operating voltage of 120 kV. About 200 different particles were analyzed to determine the size distribution and the mean size of nanoparticles using ImageJ. Dynamic light scattering (DLS) and zeta potential measurements were performed with a Zetasizer Nano ZS (Malvern) with a He/Ne 633 nm laser at 25 °C. For each sample, three independent measurements were performed. Finally, the optical properties of gold nanoparticles were studied by UV-Vis spectroscopy using a Varian Cary 5000 UV-Vis-NIR spectrophotometer.

C. elegans growth/exposure

C. elegans were grown in NGM agar seeded with *E. coli* OP50 at 20^oC. In the acute treatment, a 48-h synchronized population was exposed for 24 h in 2 mL of 50% M9 buffer at 100 and 500 µg/mL Cit- and BSA-SPIONs, and at 100 µg/mL 11-nm Au-NPs. In the prolonged treatment setting, a synchronized population was exposed from L1 for 48 h in NGM agar plates with food supplemented with 100 µg/ml Cit- and BSA-SPIONs. A minimum of 2000 animals were exposed per each sample in triplicate.

RNA extraction

Total RNA was extracted using Tri-reagent (Biomatik) as recommended by the manufacturer, including an additional initial vortexing step (3 min) with equal quantity of acid-washed glass beads than worm pellet (Sigma). The total concentration of RNA was quantified using a Nanodrop ND1000 spectrometer (Thermo Scientific) and the quality of the RNA was analyzed by 0.8% agarose gel electrophoresis to determine RNA integrity and absence of

genomic DNA carry over. An additional quality control was performed by analyzing the RNA of all samples via the bioanalyzer platform (Agilent Genomics). No differences in terms of purity, integrity and quantity of the RNA was observed from RNA isolated from control or treated worms.

qPCR

cDNA was synthesized with 1000 ng of RNA by means of an oligo-dT primer. The cDNA purity and concentration was assessed using a Nanodrop spectrophotometer. qPCR was carried out using the ABI Prism 7500 FAST platform (Applied BioSystems). All probes were acquired from the Universal ProbeLibrary (Roche Applied Science) and primers were designed to be intron-spanning (Table S1). For each qPCR reaction, a mastermix was prepared containing of 5 µL ROX (Roche), 0.1 µL of probe (10 µM), 0.4 µL of each primer (10 pM) and completed with RNAse-free water to a final volume of 8.8 µL. Using standard ABI Prism cycling conditions (2 min at 50 °C, followed by 10 min at 95 °C, and 40 cycles of 15 s at 95 °C and 1 min at 60 °C), C_T (threshold cycle) values were determined. Data analysis was performed using the ABI 7000 system software, and the ΔΔCT method was used to calculate the fold change in gene expression. Gene expression was normalized to the house-keeping gene *rla-1*, which encodes an acidic ribosomal subunit protein P1.(Swain *et al.*, 2004, Swain *et al.*, 2010) qPCR quantifications were performed on samples from three independent experiments; four technical replicates were analyzed for each.

Microarrays

The transcriptomic analysis was performed using Affymetrix *C. elegans* microarrays in triplicate for: untreated worms; worms treated with 500 µg/ml Cit-SPIONs; worms treated with 500 µg/ml BSA-SPIONs. The exposure conditions were 24 h exposure in 50% M9 buffer at 20 ^{o}C. The expression levels of treated and untreated worms were compared, and their relative fold change was determined. Fourteen genes were quantitatively assessed by qPCR to validate the microarray experiments using the primers and probes are indicated in Table S1. They were selected from a list of 75 most differentially expressed genes ($p<0.01$, either up- or down-regulated) following an exposure to Cit-SPION (Table S2), namely *vit-1*, *col-179*, *skr-7*, *F59A6.10*, *R12B2.8*, *F32A7.8*, *nlp-37*, *scl-22*, *cul-3*, *hrp-2*, *F55G11.8*, *F35E12.8*, cyp-*13A5*, and *F49F1.5*. The analysis of the results was performed using two bioinformatics resources: DAVID was used to identify molecular pathways affected by NP exposure studying differentially expressed genes,(Huang da *et al.*, 2009b) and PANTHER was used to classify the most significant responses according to their biological function and the molecular process in which they were involved.(Mi *et al.*, 2016)

The microarray data has been submitted to the National Center for Biotechnology Information's (NCBI) Gene Expression Omnibus (GEO) database (http://www.ncbi.nlm.nih.gov/geo), accession numbers GSE93188 (C-SPIONs) and GSE93186 (BSA-SPIONs).

Synchrotron Fourier Transform infrared microscopy (SR-μFTIR)

We exposed ~500 late L3 worms to 50% M9 buffer (control animals) or to 500 μg/ml Cit-SPIONs in 50% M9 buffer (treated animals) for 24 h at 20 ^{o}C. After exposure, worms were washed three times with MilliQ water, transferred to a CaF_2 window (~50/worms per slide) and dried in vacuum conditions. SR-μFTIR experiments were performed at the MIRAS beamline at ALBA synchrotron, Spain using a Hyperion 3000 Microscope coupled to a Vertex 80 spectrometer (Brucker) equipped with 36x magnification objective. The measuring range was 900−4000 cm^{-1} and the spectra collection was done in transmission mode at 4 cm^{-1} spectral resolution, 8 μm × 8 μm aperture dimensions using a MCT detector. For each spectrum 128 scans were co-added. FTIR spectra were acquired in 10 different worms at 6-8 different locations per worm. Background spectra were collected from a clean area of each CaF_2 window.

FTIR data was analyzed using OPUS 7.5 (Brucker) and Origin 9.1. The spectra exhibiting strong Mie scattering were eliminated and second derivative of the spectra was applied in order to eliminate the baseline and improve the resolution of the different bands using a Savitsky−Golay algorithm with a 15-point filter and a polynomial order of two. The derivative of each FTIR spectrum was computed and the ratio corresponding to lipid oxidation 1741 cm^{-1} /2960 cm^{-1} (COOH/$-CH_3$) was calculated.(Benseny-Cases *et al.*, 2014)

Statistical analysis

Past 3.03 was used for all statistical analyzes. Statistical significance between two groups was assessed by T tests. Three levels of statistical significance were considered in all cases: * $p < 0.05$; ** $p < 0.01$; *** $p < 0.005$.

Results

Tested materials

Citrate-coated SPIONs (hereinafter referred to as Cit-SPIONs) were produced by microwave-assisted thermal decomposition and characterized by TEM, DLS, and zeta potential. Cit-SPIONs had a TEM diameter of 5.6 ± 0.8 nm, a hydrodynamic mean diameter of 17 nm (15% polydispersity) and a zeta potential of –41 ± 8 mV. Bovine serum albumin coated SPIONs (BSA-SPIONs) were prepared by a pH-adjusted BSA adsorption protocol.(Yu *et al.*, 2014) They had a hydrodynamic mean diameter of 25 nm (19% polydispersity) and a zeta potential of –26

± 9 mV. TEM observations performed with negative staining confirmed an increase of 7 nm in diameter, supporting the formation of a BSA monolayer coating around the SPION core.(Yu *et al.*, 2014, Yu *et al.*, 2016b) The characterization of materials is presented in Figure S1.

Selection of exposure doses

The doses of exposure were selected based on their lethality to *C. elegans*. 100 µg/ml SPIONs, which is close to the LC10, was chosen as a biocompatible dose to investigate mechanisms in a low nanotoxic conditions. In addition, 500 µg/ml was selected which is a dose that is close to the LC50, with the aim to define the molecular responses during a harsh nanotoxic challenge. Notably, the latter dose (associated with high lethality) could not be investigated in higher model organisms due to ethical concerns, hence the use of an invertebrate model contributes to a better understanding of potential threats under highly toxic conditions. Having said that, it is difficult to compare NP uptake in *C. elegans* with human exposure given the different modes of administration (oral *versus* intravenous), and we anticipate that the human dosing regime is at last 1 order of magnitude below the exposure concentrations applied in this present study. The reader is referred to previous work for a broader characterization of the toxicological effects of the test materials in *C. elegans*.(Gonzalez-Moragas *et al.*, 2015b)

Genome-wide study by microarrays

We performed a transcriptomic analysis by microarrays in triplicate of worms acutely exposed (24 h) to 500 µg/ml SPION, a dose close to the LC_{50}, to investigate the molecular mechanisms underlying harmful effects. The expression levels of treated worms were compared to that of untreated worms and their relative fold change was determined. We validated the microarray experiments performing qPCR of the 14 most differentially expressed genes following an exposure to Cit-SPIONs (Table S3). Based on the microarray experiments, Cit-SPION or BSA-coated treatment changed significantly ($p<0.01$) the expression of 1095 or 2165 transcripts, respectively, while only 308 genes were significantly affected by both treatments (Figure 1 and Tables S3–S5). The molecular functions and biological processes of these genes were analyzed using PANTHER bioinformatic tool (Figure S2).(Mi *et al.*, 2013, Mi *et al.*, 2016)

Pathway Enrichment Test was performed using the DAVID bioinformatics tool to determine which molecular pathways were affected by Cit-SPIONs only, BSA-SPIONs only or both SPIONs (Figure 1).(Huang da *et al.*, 2009a, Huang da *et al.*, 2009b) Both SPIONs affected several essential pathways for processing environmental information involved in signal transduction, namely Wnt, MAPK and Calcium (Ca) signaling pathways. Cit-SPIONs also affected the transcription of other signal transduction pathways including TFG-beta or ErbB, and genetic information processing routes, in particular RNA transport and protein processing in the endoplasmic reticulum (ER). In contrast, BSA-SPIONs predominantly affected metabolic

mechanisms, among them xenobiotic biodegradation by cytochrome P450, and also genetic information processing pathways (proteasome, spliceosome and mRNA surveillance pathway). The lysosomal/endocytic pathway was disturbed by both SPIONs to a similar extent.

We also analyzed the expression of several *C. elegans* genes which are orthologous to mammalian genes encoding albumin receptors known to bind specifically to albumin and mediate the entrance of albumin-coated nanoparticles by active transport.(Merlot *et al.*, 2014) Among them, we studied *C. elegans ost-1* which encodes SPARC, *crt-1* which encodes calreticulin and *ZC116.3* which hypothetically encodes cubilin. We compared Cit- and BSA-SPIONs expression levels and did not observe significant differences, however we do not exclude the potential role of these receptors at lower doses or after prolonged treatment.

Study of selected genes by qPCR

We quantitatively evaluated by qPCR the transcription of fourteen strongly differentially expressed genes identified in the microarray experiments as to Cit-SPIONs at 500 µg/ml, which allowed us to validate the microarray results. Among these genes, eight were selected for follow-up experiments based on their well-documented biological functions in WormBase.(Howe *et al.*, 2016) They were involved in innate immune response (*col-179*, *F44G11.8*, *F35E12.8*), oxidative metabolism (*cyp-13A5*), apoptosis (*F49F1.5*), ubiquitination (*cul-3*), neurosignaling (*nlp-37*), and body morphogenesis (*skr-7*). We also investigated genes previously linked to nanotoxicity in *C. elegans* involved in metal detoxification (*mtl-1*, *mtl-2*, *pcs-1*), oxidative stress (*sod-2*, *sod-3*), iron homeostasis (*ftn-1*, *ftn-2*, *smf-3*), intestinal morphogenesis (*act-5*, *eps-8*, *elt-2*), and endocytosis (*chc-1*, *dyn-1*, *eps-8*) (see Table 1 for a more detailed description of gene function).(Tsyusko *et al.*, 2012, Quach *et al.*, 2013, Polak *et al.*, 2014) We evaluated the gene expression of *C. elegans* exposed for 24 h to 100 and 500 µg/ml Cit- and BSA-SPIONs in 50% M9 buffer, doses which approximate the LC_{10} and LC_{50}, respectively.(Gonzalez-Moragas *et al.*, 2015b)

The gene expression in worms acutely exposed to 100 µg/ml of BSA-SPION was, in general, closer to the control animals than worms treated with Cit-SPION (Table 2 and Figure S3). In contrast, an acute incubation to 500 µg/ml resulted in similar gene expression levels, irrespectively of the coating. Regarding the most differentially expressed genes (identified in the microarray experiments for Cit-SPIONs at 500 µg/ml), a low dose of Cit-SPIONs activated the innate immune system and oxidative metabolism to a greater extent than BSA-SPIONs, whilst at the higher dose the response was less coating-dependent. One exception was *cul-3*, a gene involved in protein degradation, which was up-regulated in worms exposed to Cit-SPIONs but not by BSA-SPIONs (Figure 2, Table 2 and Figure S4). Focusing on genes previously linked to nanotoxicity (Figure 3), exposure to SPIONs either at 100 or 500 µg/ml suppressed the

antioxidant and metal detoxification pathways, and inhibited the neurosignaling peptide *nlp-37*. It is conceivable that *nlp-37* might be involved in SPION-induced neurotoxicity in *C. elegans*, however additional markers would be required to confirm this finding.(Li *et al.*, 2012a, Wu *et al.*, 2015, Scharf *et al.*, 2016) SPION exposure also modulated the expression of clathrin and dynamin, suggesting that SPIONs are taken up via endocytosis, which aligns well with previously reported results.(Tsyusko *et al.*, 2012, Li *et al.*, 2015) SPIONs also exerted significant effects on the expression of genes involved in the structure and integrity of the intestinal barrier (*act-5, eps-8* and *elt-2*). These effects were not dose-dependent in the case of Cit-SPIONs, while responses were generally amplified at the higher dose of BSA-SPION (Table 2). The analysis of the iron homeostasis genes revealed that exposure to either SPIONs led to ferritin up-regulation and divalent metal ion transporter *smf-3* down-regulation.

Prolonged vs. acute exposures

The transcriptional response of the genes frequently linked to nanotoxicity was also investigated in worms exposed for 48h on NGM plates with food to a dose equivalent to 100 µg/ml SPIONs (prolonged exposure). Under those conditions, Cit-SPIONs induced more significant responses than BSA-SPIONs comparing to untreated worms, which only affected metallothioneins and ferritin and exerted little or no effects on the endocytosis/intestinal genes (Figure 4A, Table 2 and Figure S2).

The effect of dose, coating and duration of exposure on the gene expression levels are summarized in Table 2.

Nanoparticle-specific effects

Gold is an inert metal, hence the effects of Au-NPs are considered to be nano-specific.(Tsyusko *et al.*, 2012, Soenen *et al.*, 2015) We evaluated the expression levels of the iron homeostasis genes after treatment of *C. elegans* with 11-nm gold nanoparticles (for their characterization see Figure S5) to determine if ferritin up-regulation could occur without iron release from the NP core, and confirmed *ftn-1* up-regulation upon acute Au-NP treatment at 100 µg/ml to a similar extent than in the case of SPIONs (Figure 4B).

Study of lipid oxidation

We measured the degree of lipid oxidation in *C. elegans* treated with Cit-SPION by SR-µFTIR to investigate the role of oxidative stress in SPION toxicity. Figure 5 shows that the band at 1741 cm^{-1}, corresponding to carbonyl groups (product of lipid oxidation reaction), is more intense in the spectra of SPION-treated *C. elegans* than in untreated animals. This band, normalized by total lipid (CH_3 groups), shows significant differences between untreated and treated animals ($p<0.01$), indicating that lipid oxidation is induced by SPION treatment.

Discussion

Pathway identification

BSA-SPIONs can be of particular interest for biomedical applications based on their enhanced colloidal stability in cell media compared to Cit-SPIONs.(Yu *et al.*, 2014) Our transcriptomic analysis in *C. elegans* revealed a coating-dependent response based on the low coincidence of genes (11%) affected by both SPION types. These results are in good agreement with *in vitro* studies concluding that even subtle modifications in NP coating can exert a substantial impact on their bio-identity.(Soenen *et al.*, 2015) Interestingly, the concurrently affected signaling pathways (Wnt, MAPK, Ca) are frequently used during metazoan development to control different biological processes and to regulate many aspects of cell identity, function, and survival in multicellular animals.(Gumienny and Savage-Dunn, Sawa and Korswagen, Sundaram) Previous studies in *C. elegans* have linked MAPK signaling pathway with oxidative stress, DNA damage and reproductive function.(Lim *et al.*, 2012, Roh *et al.*, 2012, Chatterjee *et al.*, 2014) Modulation of intracellular Ca levels and Ca signaling have been frequently linked to nanotoxicity, leading to cell necrosis and ultimately mortality.(AshaRani *et al.*, 2009, Huang *et al.*, 2010, Tsyusko *et al.*, 2012) Besides these mechanisms, Cit-SPIONs affected the endoplasmic reticulum function, which may indicate activation of unfolded protein response.(Tsyusko et al., 2012) Conversely, BSA-SPIONs triggered the xenobiotic detoxification enzyme cytochrome P450, which have been also reported to be differentially expressed in *C. elegans* exposed to TiO_2 and CeO_2-NPs.(Roh *et al.*, 2010a, Helvenstein *et al.*, 2015, Rocheleau *et al.*, 2015, Iavicoli *et al.*, 2016) NP-induced responses on protein processing and proteasome have been previously linked to nanotoxicity of inorganic nanoparticles. In particular, Scharf *et al.* found that protein homeostasis was a major target of SiO_2-NPs.(Scharf *et al.*, 2016) The similar effect of both SPIONs on the lysosomal compartment suggests that this 'dustbin' organelle might be part of the cellular NP detoxifying mechanism, consistent with previous reports that endosome formation is an instrumental component of NP toxicity *in vivo*.(Tsyusko *et al.*, 2012, Maurer *et al.*, 2016, Zhang *et al.*, 2016)

Evaluation of specific molecular markers

The single-gene analyses by qPCR revealed that the protein coating reduced the biological responses triggered by SPIONs at low doses, whereas similar responses for both SPIONs were observed at higher doses at which more general toxicity mechanisms might prevail. The effects of SPIONs on antioxidant and metal detoxification genes support the belief that oxidative stress and metal toxicity form an integral part of the biological response cascade in SPION treated *C. elegans*, however the lack of a strong dose-response relationship in these pathways suggest they may not be the main mechanism that drives the nanotoxicity. Given that

endocytosis pathways were affected by acute treatment, it suggests that SPIONs may possibly be internalized by intestinal cells via endocytosis. However, SPIONs also triggered a response of intestinal-related genes which might indicate that the proximity of the luminal NPs to the microvilli can influence microvilar structure and its remodeling processes. Although SPIONs did not cause intestinal cytotoxicity or structural damage at 24 hours,(Yu *et al.*, 2016a) we do not discard that a prolonged contact with NPs could lead to irreversible damage on the intestinal barrier.(Zhao *et al.*, 2014) Ferritin up-regulation occurred after SPION and Au-NP treatment, and similar effects were observed after *C. elegans* exposure to arsenic, cadmium and ethosuximide.(Chen *et al.*, 2013, Chen *et al.*, 2015, Petryszak *et al.*, 2016) Hence, the effects of SPIONs in iron homeostasis might be part of a more general response to toxicants and not necessarily linked to oxidative dissolution of the SPION core into free iron.

The role of oxidative stress

Oxidative stress was not identified in the transcriptomic analysis, however qPCR confirmed the responsiveness of selected antioxidant pathways to SPIONs. In addition, ferritin up-regulation is not restricted to activation by free iron, which is scarcely released from SPIONs especially in the BSA-coated ones.(Gonzalez-Moragas *et al.*, 2015b) Hence, we believe ferritin activation predominantly occurs via the electrophile response element due to elevated production of reactive oxygen species induced by SPION treatment.(Tsuji *et al.*, 2000) Indeed, the SR-μFTIR experiments provided further evidence of oxidative stress in *C. elegans* challenged with SPIONs, confirming significantly higher lipid oxidation levels in NP-treated animals.

Predicted model of SPION toxicity

Our investigations suggest that SPIONs can cross the intestinal barrier of *C. elegans* possibly via clathrin-mediated endocytosis, activating endocytic/lysosomal pathways. These findings are consistent with previous observations by electron microscopy, however further genetic and biochemical experimentation is required to confirm the internalization hypothesis.(Yu *et al.*, 2016a) We report affectation of key signal transduction pathways (MAPK, Wnt and Ca signaling) and responsiveness of several biological cascades, including innate immune responses, metal detoxification and oxidative stress pathways. The deregulation of the defense/compensation mechanisms against NPs has the potential to disrupt key biological processes and finally result in premature death.(Roh *et al.*, 2010b, Tsyusko *et al.*, 2012, Ahn *et al.*, 2014) These biological mechanisms have been previously reported in *C. elegans* for a range of inorganic NPs.(Kim *et al.*, 2012, Li *et al.*, 2012b, Lim *et al.*, 2012, Wu *et al.*, 2012, Rui *et al.*, 2013, Wu *et al.*, 2013, Ahn *et al.*, 2014, Polak *et al.*, 2014) The effects of the activated pathways might be of importance in the long term, hence further investigation is required to correlate the pathways identified in this work with the effects of chronic exposures in *C. elegans*.

Pathway enrichment analysis revealed coating-dependent affectation of molecular mechanisms, indicative of a different bio-identity of Cit-SPIONs and BSA-SPIONs *in vivo*.(Yu *et al.*, 2016a). qPCR experiments showed that the pre-formed protein corona of the BSA-SPIONs mitigated the harmful effects compared to Cit-SPIONs, especially at low doses. Moreover, lower biological impact was detected after prolonged exposure to BSA-SPIONs, based on gene expression levels closer to that of untreated animals. Taken together, our findings suggest that BSA acts as a biomimetic layer that reduces SPION dissolution *in vivo* and shields the interaction of the nanoparticle core with the intestinal cells,(Geppert *et al.*, 2012, Gonzalez-Moragas *et al.*, 2015b) thereby minimizing SPION adverse effects in *C. elegans*. Therefore, BSA-SPIONs could be better suited for biomedical applications than Cit-SPIONs, allowing drug loading in the protein coating and offering promising functionalization possibilities.(Laurent et al., 2010, Liu et al., 2013). Figure 6 illustrates the biological responses detected upon Cit- and BSA-SPIONs treatment in *C. elegans*.

Conclusions

C. elegans is a good model organism to investigate the bio-identity of nanoparticles *in vivo*. Here we evaluated the responses of *C. elegans* challenged with SPIONs with different surface coatings (protein *vs.* citrate) and confirmed the role of several molecular mechanisms frequently related with nanotoxicity. In particular, we show the role of oxidative stress in SPION-treated *C. elegans* by gene expression analysis and by synchrotron FTIR microscopy. Despite the role of oxidative stress, according to the transcriptomic analysis the major contributors to SPION toxicity are several key signaling transduction pathways, including Wnt, MAPK and Calcium pathways, which may also govern the response of *C. elegans* to other metal or metal oxide NPs.

By identifying the molecular mechanisms responsible for the biological responses observed after NP exposure, and the related physicochemical characteristics of NPs, we will be able to understand and predict the *in vivo* behavior of NPs and optimize their design towards low-toxic and safe nanomaterials for human use. This work combines genomics with single gene evaluations, and in doing so expands our knowledgebase of the mechanistic effects of inorganic nanoparticles *in vivo*, which to date is a largely unexplored field. We believe our results can contribute to guide further experiments in higher model organisms.

Declaration of interest

The authors report no conflicts of interest.

Acknowledgements

C. elegans N2 and *E. coli* OP50 were provided by the CGC, which is funded by NIH Office of Research Infrastructure Programs (P40 OD010440). This research was partially funded by the Spanish Ministry of Economy and Competitiveness co-funded by European Social Funds, through project MAT2015-64442-R, the 'Severo Ochoa' Program for Centers of Excellence in R&D (SEV- 2015-0496), the Ramon y Cajal program (AL, RyC-2010-06082) and FPU program (LGM, FPU12/05549), the Generalitat de Catalunya (2014SGR213), People Program of the European Commission (grant agreement no. 303630, co-funded by the European Social Fund), the COST Action GENIE (Action No. BM1408-A). We acknowledge Víctor Fuentes for his collaboration in the synthesis of gold nanoparticles. SRS acknowledges core funding from King's College London and access and support from the King's Genomics Centre. SR-μFTIR experiments were performed at MIRAS beamline at ALBA Synchrotron with the collaboration of ALBA staff.

References

Aardema, M.J. & Macgregor, J.T., 2002. Toxicology and genetic toxicology in the new era of "toxicogenomics": impact of "-omics" technologies. *Mutation Research-Fundamental and Molecular Mechanisms of Mutagenesis,* 499**,** 13-25.

Ahn, J.-M., Eom, H.-J., Yang, X., Meyer, J.N. & Choi, J., 2014. Comparative toxicity of silver nanoparticles on oxidative stress and DNA damage in the nematode, Caenorhabditis elegans. *Chemosphere,* 108**,** 343-352.

Asharani, P.V., Hande, M.P. & Valiyaveettil, S., 2009. Anti-proliferative activity of silver nanoparticles. *Bmc Cell Biology,* 10.

Benseny-Cases, N., Klementieva, O., Cotte, M., Ferrer, I. & Cladera, J., 2014. Microspectroscopy (μFTIR) Reveals Co-localization of Lipid Oxidation and Amyloid Plaques in Human Alzheimer Disease Brains. *Analytical Chemistry,* 86**,** 12047-12054.

Chatterjee, N., Eom, H.J. & Choi, J., 2014. Effects of silver nanoparticles on oxidative DNA damage–repair as a function of p38 MAPK status: A comparative approach using human Jurkat T cells and the nematode Caenorhabditis elegans. *Environmental and Molecular Mutagenesis,* 55**,** 122-133.

Chen, P., Martinez-Finley, E.J., Bornhorst, J., Chakraborty, S. & Aschner, M., 2013. Metal-induced neurodegeneration in *C. elegans*. *Frontiers in Aging Neuroscience,* 5.

Chen, X., Mccue, H.V., Wong, S.Q., Kashyap, S.S., Kraemer, B.C., Barclay, J.W., Burgoyne, R.D. & Morgan, A., 2015. Ethosuximide ameliorates neurodegenerative disease phenotypes by modulating DAF-16/FOXO target gene expression. *Molecular Neurodegeneration,* 10**,** 51.

Elingarami, S., Li, X. & He, N., 2013. Applications of Nanotechnology, Next Generation Sequencing and Microarrays in Biomedical Research. *Journal of Nanoscience and Nanotechnology,* 13**,** 4539-4551.

Frens, G., 1973. Controlled Nucleation for the Regulation of the Particle Size in Monodisperse Gold Suspensions. *Nature Physical Science,* 241**,** 20-22.

Geppert, M., Hohnholt, M.C., Nürnberger, S. & Dringen, R., 2012. Ferritin up-regulation and transient ROS production in cultured brain astrocytes after loading with iron oxide nanoparticles. *Acta Biomaterialia,* 8**,** 3832-3839.

Gonzalez-Moragas, L., Roig, A. & Laromaine, A., 2015a. *C. elegans* as a tool for in vivo nanoparticle assessment. *Advances in Colloid and Interface Science,* 219**,** 10-26.

Gonzalez-Moragas, L., Yu, S.-M., Carenza, E., Laromaine, A. & Roig, A., 2015b. Protective Effects of Bovine Serum Albumin on Superparamagnetic Iron Oxide Nanoparticles Evaluated in the Nematode Caenorhabditis elegans. *ACS Biomaterials Science & Engineering,* 1**,** 1129-1138.

Gumienny, T.L. & Savage-Dunn, C., TGF-β signaling in *C. elegans*. *In* T.C.E.R. Community (ed.) *WormBook.* WormBook.

Helvenstein, M., Stanicki, D., Laurent, S. & Blankert, B., 2015. Interaction between Iron Oxide Nanoparticles and HepaRG Cells: A Preliminary In Vitro Evaluation. *Journal of Nanomaterials,* 2015**,** 9.

Howe, K.L., Bolt, B.J., Cain, S., Chan, J., Chen, W.J., Davis, P., Done, J., Down, T., Gao, S., Grove, C., Harris, T.W., Kishore, R., Lee, R., Lomax, J., Li, Y., Muller, H.-M., Nakamura, C., Nuin, P., Paulini, M., Raciti, D., Schindelman, G., Stanley, E., Tuli, M.A., Van auken, K., Wang, D., Wang, X., Williams, G., Wright, A., Yook, K., Berriman, M., Kersey, P., Schedl, T., Stein, L. & Sternberg, P.W., 2016. WormBase 2016: expanding to enable helminth genomic research. *Nucleic Acids Research,* 44**,** D774-D780.

Huang, C.-C., Aronstam, R.S., Chen, D.-R. & Huang, Y.-W., 2010. Oxidative stress, calcium homeostasis, and altered gene expression in human lung epithelial cells exposed to ZnO nanoparticles. *Toxicology in Vitro,* 24**,** 45-55.

Huang Da, W., Sherman, B.T. & Lempicki, R.A., 2009a. Bioinformatics enrichment tools: paths toward the comprehensive functional analysis of large gene lists. *Nucleic Acids Res,* 37**,** 1-13.

Huang Da, W., Sherman, B.T. & Lempicki, R.A., 2009b. Systematic and integrative analysis of large gene lists using DAVID bioinformatics resources. *Nat Protoc,* 4**,** 44-57.

Iavicoli, I., Leso, V. & Schulte, P.A., 2016. Biomarkers of susceptibility: State of the art and implications for occupational exposure to engineered nanomaterials. *Toxicology and Applied Pharmacology,* 299**,** 112-124.

Kim, S.W., Nam, S.-H. & An, Y.-J., 2012. Interaction of Silver Nanoparticles with Biological Surfaces of Caenorhabditis elegans. *Ecotoxicology and Environmental Safety,* 77**,** 64-70.

Krug, H.F., 2014. Nanosafety Research-Are We on the Right Track? *Angewandte Chemie-International Edition,* 53**,** 12304-12319.

Lehner, B., 2013. Genotype to phenotype: lessons from model organisms for human genetics. *Nat Rev Genet,* 14**,** 168-178.

Li, L., Wan, T., Wan, M., Liu, B., Cheng, R. & Zhang, R.Y., 2015. The effect of the size of fluorescent dextran on its endocytic pathway. *Cell Biology International,* 39**,** 531-539.

Li, Y., Yu, S., Wu, Q., Tang, M., Pu, Y. & Wang, D., 2012a. Chronic Al2O3-nanoparticle exposure causes neurotoxic effects on locomotion behaviors by inducing severe ROS production and disruption of ROS defense mechanisms in nematode Caenorhabditis elegans. *Journal of Hazardous Materials,* 219**,** 221-230.

Li, Y., Yu, S., Wu, Q., Tang, M., Pu, Y. & Wang, D., 2012b. Chronic Al2O3-nanoparticle exposure causes neurotoxic effects on locomotion behaviors by inducing severe ROS production and disruption of ROS defense mechanisms in nematode Caenorhabditis elegans. *J Hazard Mater,* 219-220**,** 221-30.

Lim, D., Roh, J.-Y., Eom, H.-J., Choi, J.-Y., Hyun, J. & Choi, J., 2012. Oxidative stress-related PMK-1 P38 MAPK activation as a mechanism for toxicity of silver nanoparticles to reproduction in the nematode Caenorhabditis elegans. *Environmental Toxicology and Chemistry,* 31**,** 585-592.

Maurer, L.L., Yang, X., Schindler, A.J., Taggart, R.K., Jiang, C., Hsu-Kim, H., Sherwood, D.R. & Meyer, J.N., 2016. Intracellular trafficking pathways in silver nanoparticle uptake and toxicity in Caenorhabditis elegans. *Nanotoxicology,* 10**,** 831-5.

Merlot, A.M., Kalinowski, D.S. & Richardson, D.R., 2014. Unraveling the mysteries of serum albumin—more than just a serum protein. *Frontiers in Physiology,* 5.

Mi, H., Muruganujan, A., Casagrande, J.T. & Thomas, P.D., 2013. Large-scale gene function analysis with the PANTHER classification system. *Nat. Protocols,* 8**,** 1551-1566.

Mi, H., Poudel, S., Muruganujan, A., Casagrande, J.T. & Thomas, P.D., 2016. PANTHER version 10: expanded protein families and functions, and analysis tools. *Nucleic Acids Res,* 44**,** D336-42.

Nuwaysir, E.F., Bittner, M., Trent, J., Barrett, J.C. & Afshari, C.A., 1999. Microarrays and toxicology: The advent of toxicogenomics. *Molecular Carcinogenesis,* 24**,** 153-159.

Ohno, Y., 2002. ICH Guidelines—Implementation of the 3Rs (Refinement, Reduction, and Replacement): Incorporating Best Scientific Practices into the Regulatory Process. *ILAR Journal,* 43**,** S95-S98.

Pareek, C.S., Smoczynski, R. & Tretyn, A., 2011. Sequencing technologies and genome sequencing. *Journal of Applied Genetics,* 52**,** 413-435.

Petryszak, R., Keays, M., Tang, Y.A., Fonseca, N.A., Barrera, E., Burdett, T., Füllgrabe, A., Fuentes, A.M.-P., Jupp, S., Koskinen, S., Mannion, O., Huerta, L., Megy, K., Snow, C., Williams, E., Barzine, M., Hastings, E., Weisser, H., Wright, J., Jaiswal, P., Huber, W., Choudhary, J., Parkinson, H.E. & Brazma, A., 2016. Expression Atlas update—an integrated database of gene and protein expression in humans, animals and plants. *Nucleic Acids Research,* 44**,** D746-D752.

Polak, N., Read, D.S., Jurkschat, K., Matzke, M., Kelly, F.J., Spurgeon, D.J. & Stuerzenbaum, S.R., 2014. Metalloproteins and phytochelatin synthase may confer protection against zinc oxide nanoparticle induced toxicity in Caenorhabditis elegans. *Comparative Biochemistry and Physiology C-Toxicology & Pharmacology,* 160**,** 75-85.

Poma, A. & Di Giorgio, M.L., 2008. Toxicogenomics to Improve Comprehension of the Mechanisms Underlying Responses of In Vitro and In Vivo Systems to Nanomaterials: A Review. *Current Genomics,* 9**,** 571-585.

Poynton, H.C., Lazorchak, J.M., Impellitteri, C.A., Blalock, B.J., Rogers, K., Allen, H.J., Loguinov, A., Heckrnan, J.L. & Govindasmawy, S., 2012. Toxicogenomic Responses of Nanotoxicity in Daphnia magna Exposed to Silver Nitrate and Coated Silver Nanoparticles. *Environmental Science & Technology,* 46**,** 6288-6296.

Quach, T.K., Chou, H.T., Wang, K., Milledge, G.Z. & Johnson, C.M., 2013. Genome-Wide Microarrray Analysis Reveals Roles for the REF-1 Family Member HLH-29 in Ferritin Synthesis and Peroxide Stress Response. *PLoS ONE,* 8**,** e59719.

Rocheleau, S., Arbour, M., Elias, M., Sunahara, G.I. & Masson, L., 2015. Toxicogenomic effects of nano- and bulk-TiO2 particles in the soil nematode Caenorhabditis elegans. *Nanotoxicology,* 9**,** 502-12.

Roh, J.-Y., Eom, H.-J. & Choi, J., 2012. Involvement of Caenohabditis elegans MAPK Signaling Pathways in Oxidative Stress Response Induced by Silver Nanoparticles Exposure. *Toxicological research,* 28**,** 19-24.

Roh, J.-Y., Park, Y.-K., Park, K. & Choi, J., 2010a. Ecotoxicological investigation of CeO2 and TiO2 nanoparticles on the soil nematode Caenorhabditis elegans using gene expression, growth, fertility, and survival as endpoints. *Environmental Toxicology and Pharmacology,* 29**,** 167-172.

Roh, J.Y., Park, Y.K., Park, K. & Choi, J., 2010b. Ecotoxicological investigation of CeO(2) and TiO(2) nanoparticles on the soil nematode Caenorhabditis elegans using gene expression, growth, fertility, and survival as endpoints. *Environ Toxicol Pharmacol,* 29**,** 167-72.

Rui, Q., Zhao, Y., Wu, Q., Tang, M. & Wang, D., 2013. Biosafety assessment of titanium dioxide nanoparticles in acutely exposed nematode Caenorhabditis elegans with mutations of genes required for oxidative stress or stress responset. *Chemosphere,* 93**,** 2289-2296.

Sawa, H. & Korswagen, H.C., Wnt signaling in *C. elegans*. *In* T.C.E.R. Community (ed.) *WormBook.* WormBook.

Scharf, A., Guhrs, K.H. & Von Mikecz, A., 2016. Anti-amyloid compounds protect from silica nanoparticle-induced neurotoxicity in the nematode *C. elegans*. *Nanotoxicology,* 10**,** 426-435.

Soenen, S.J., Parak, W.J., Rejman, J. & Manshian, B., 2015. (Intra)Cellular Stability of Inorganic Nanoparticles: Effects on Cytotoxicity, Particle Functionality, and Biomedical Applications. *Chemical Reviews,* 115**,** 2109-2135.

Soenen, S.J., Rivera-Gil, P., Montenegro, J.-M., Parak, W.J., De Smedt, S.C. & Braeckmans, K., 2011. Cellular toxicity of inorganic nanoparticles: Common aspects and guidelines for improved nanotoxicity evaluation. *Nano Today,* 6**,** 446-465.

Starnes, D.L., Lichtenberg, S.S., Unrine, J.M., Starnes, C.P., Oostveen, E.K., Lowry, G.V., Bertsch, P.M. & Tsyusko, O.V., 2016. Distinct transcriptomic responses of Caenorhabditis elegans to pristine and sulfidized silver nanoparticles. *Environmental pollution (Barking, Essex : 1987),* 213**,** 314-21.

Sundaram, M.V., RTK/Ras/MAPK signaling. *In* T.C.E.R. Community (ed.) *WormBook.* WormBook.

Swain, S., Wren, J.F., Sturzenbaum, S.R., Kille, P., Morgan, A.J., Jager, T., Jonker, M.J., Hankard, P.K., Svendsen, C., Owen, J., Hedley, B.A., Blaxter, M. & Spurgeon, D.J., 2010. Linking toxicant physiological mode of action with induced gene expression changes in Caenorhabditis elegans. *BMC Syst Biol,* 4**,** 32.

Swain, S.C., Keusekotten, K., Baumeister, R. & Sturzenbaum, S.R., 2004. *C. elegans* metallothioneins: new insights into the phenotypic effects of cadmium toxicosis. *J Mol Biol,* 341**,** 951-59.

Teeguarden, J.G., Mikheev, V.B., Minard, K.R., Forsythe, W.C., Wang, W., Sharma, G., Karin, N., Tilton, S.C., Waters, K.M., Asgharian, B., Price, O.R., Pounds, J.G. & Thrall, B.D., 2014. Comparative iron oxide nanoparticle cellular dosimetry and response in mice by the inhalation and liquid cell culture exposure routes. *Particle and Fibre Toxicology,* 11.

Truong, L., Tilton, S.C., Zaikova, T., Richman, E., Waters, K.M., Hutchison, J.E. & Tanguay, R.L., 2013. Surface functionalities of gold nanoparticles impact embryonic gene expression responses. *Nanotoxicology,* 7**,** 192-201.

Tsuji, Y., Ayaki, H., Whitman, S.P., Morrow, C.S., Torti, S.V. & Torti, F.M., 2000. Coordinate Transcriptional and Translational Regulation of Ferritin in Response to Oxidative Stress. *Molecular and Cellular Biology,* 20**,** 5818-5827.

Tsyusko, O.V., Unrine, J.M., Spurgeon, D., Blalock, E., Starnes, D., Tseng, M., Joice, G. & Bertsch, P.M., 2012. Toxicogenomic Responses of the Model Organism Caenorhabditis elegans to Gold Nanoparticles. *Environmental Science & Technology,* 46**,** 4115-4124.

Turkevich, J., Stevenson, P.C. & Hillier, J., 1951. A study of the nucleation and growth processes in the synthesis of colloidal gold. *Discussions of the Faraday Society,* 11**,** 55-75.

Wu, Q., Li, Y., Tang, M. & Wang, D., 2012. Evaluation of environmental safety concentrations of DMSA Coated Fe2O3-NPs using different assay systems in nematode Caenorhabditis elegans. *Plos One,* 7**,** e43729.

Wu, Q., Nouara, A., Li, Y., Zhang, M., Wang, W., Tang, M., Ye, B., Ding, J. & Wang, D., 2013. Comparison of toxicities from three metal oxide nanoparticles at environmental relevant concentrations in nematode Caenorhabditis elegans. *Chemosphere,* 90**,** 1123-31.

Wu, T., He, K., Zhan, Q., Ang, S., Ying, J., Zhang, S., Zhang, T., Xue, Y. & Tang, M., 2015. MPA-capped CdTe quantum dots exposure causes neurotoxic effects in nematode Caenorhabditis elegans by affecting the transporters and receptors of glutamate, serotonin and dopamine at the genetic level, or by increasing ROS, or both. *Nanoscale,* 7**,** 20460-20473.

Yu, S.-M., Gonzalez-Moragas, L., Milla, M., Kolovou, A., Santarella-Mellwig, R., Schwab, Y., Laromaine, A. & Roig, A., 2016a. Bio-identity and fate of albumin-coated SPIONs evaluated in cells and by the *C. elegans* model. *Acta Biomaterialia,* 43**,** 348-357.

Yu, S.-M., Laromaine, A. & Roig, A., 2014. Enhanced stability of superparamagnetic iron oxide nanoparticles in biological media using a pH adjusted-BSA adsorption protocol. *Journal of Nanoparticle Research,* 16**,** 2484.

Yu, S., Peralvarez-Marin, A., Minelli, C., Faraudo, J., Roig, A. & Laromaine, A., 2016b. Albumin-coated SPIONs: an experimental and theoretical evaluation of protein conformation, binding affinity and competition with serum proteins. *Nanoscale,* 8**,** 14393-14405.

Zhang, X., Zhang, H., Liang, X., Zhang, J., Tao, W., Zhu, X., Chang, D., Zeng, X., Liu, G. & Mei, L., 2016. Iron Oxide Nanoparticles Induce Autophagosome Accumulation through Multiple Mechanisms: Lysosome Impairment, Mitochondrial Damage, and ER Stress. *Molecular Pharmaceutics,* 13**,** 2578-2587.

Zhao, Y., Wu, Q., Li, Y. & Wang, D., 2013. Translocation, transfer, and in vivo safety evaluation of engineered nanomaterials in the non-mammalian alternative toxicity assay model of nematode Caenorhabditis elegans. *Rsc Advances,* 3**,** 5741-5757.

Zhao, Y., Wu, Q., Tang, M. & Wang, D., 2014. The in vivo underlying mechanism for recovery response formation in nano-titanium dioxide exposed Caenorhabditis elegans after transfer to the normal condition. *Nanomedicine-Nanotechnology Biology and Medicine,* 10**,** 89-98.

Tables

Table 1. Selected genes evaluated by qPCR.

Gene	Protein	Function
SPION-responsive genes		
col-179	Collagen	Involved in defence response to Gram-negative bacterium, innate immune response and lipid storage. Structural constituent of cuticle.
skr-7	SKp1 Related (ubiquitin ligase complex component)	Required for posterior body morphogenesis, embryonic and larval development, and cell proliferation.
cul-3	Cullin	Ubiquitination and degradation of target proteins. Expressed in many somatic tissues, including the pharynx, intestine, hypodermis, and several different muscle types.
nlp-37	Neuropeptide-Like Protein	Expressed in the virR, virL, rect_VR, rect_VL, rect_D, certain interneurons, certain sensory neurons, arcade cell, and certain head motor neurons.
F55G11.8	Ortholog of human EPHX1 (epoxide hydrolase 1, microsomal (xenobiotic))	Involved in innate immune response.
F35E12.8	Cub (CUB) Like Domain containing protein	Involved in innate immune response.
cyp-13A5	Putative Cytochrome P450 CYP13A5	Membrane-associated, heme-containing NADPH-dependent monooxygenases that catalyze the oxidative metabolism of a variety of exogenous compounds and endogenous substrates.
F49F1.5	Hypothetical protein	Engulfment of apoptotic cells.
Genes linked to nanotoxicity		
mlt-1, mlt-2	Metallothioneins	Metal detoxification and homeostasis. Stress adaptation.
pcs-1	Phytochelatin synthase	Detoxification of heavy metals.
sod-2, sod-3	Superoxide dismutase	Defence against oxidative stress.
ftn-1, ftn-2	Ferritins	Iron storage.
smf-3	Divalent metal ion transporter	Divalent metal ion transporter.
chc-1	Clathrin heavy chain	Clathrin-mediated endocytosis.
dyn-1	Dynamin	Endocytosis, synaptic vesicle recycling, cytokinesis and degradation of apoptotic cells.
act-5	Actin	Formation of the terminal web and microvilli on the apical surface of intestinal cells.
eps-8	Cell signaling adaptor protein	Epidermal and intestinal cells morphogenesis. Endocytosis.
elt-2	GATA-type transcription factor	Terminal differentiation of the intestine. Regulation of the intestinal innate immune response.

Table 2. Statistical analysis of the dose- and coating-dependent relationship in the expression levels of A) genes responsive to Cit-SPIONs, and B) pathways frequently linked to nanotoxicity. T tests were used to compare the pairs of samples and determine the *p* value. * $p < 0.05$; ** $p < 0.01$; *** $p < 0.005$.

A	**Innate immune response**			**Xenobiotic metabolism**	**Apoptosis**	**Ubiquitination**	**Neurosignaling**	**Morphogenesis**
	col-179	*F55G11.8*	*F35E12.8*	*cyp-13A5*	*F49F1.5*	*cul-3*	*nlp-37*	*skr-7*
Dose-dependence (100 µg/ml *v.s.* 500 µg/ml)								
Cit Acute	***	***	N.S.	N.S.	***	***	N.S.	***
BSA Acute	***	*	***	*	***	N.S.	*	***
Coating-dependence (Cit *v.s.* BSA)								
100 µg/ml Acute	*	*	***	N.S.	***	*	*	N.S.
500 µg/ml Acute	N.S.	*	*	***	N.S.	**	N.S.	N.S.

B		**Metal detoxification**			**Antioxidant response**		**Iron homeostasis**			**Intestinal-related genes**				
NP type	**Regime**	*mlt-1*	*mlt-2*	*pcs-1*	*sod-2*	*sod-3*	*ftn-1*	*ftn-2*	*smf-3*	*chc-1*	*dyn-1*	*eps-8*	*act-5*	*elt-2*
Dose-dependence (100 µg/ml *v.s.* 500 µg/m)														
Cit	Acute	N.S.	*	***	***	N.S.	***	***	***	N.S.	N.S.	N.S.	***	*
BSA	Acute	**	N.S.	N.S.	*	*	*	*	N.S.	***	**	**	*	N.S.
Coating-dependence (Cit *v.s.* BSA)														
100 µg/ml	Acute	*	N.S.	*	N.S.	N.S.	**	***	**	**	N.S.	N.S.	***	*
500 µg/ml	Acute	N.S.	**	*	N.S.	N.S.	N.S.	*	***	***	*	N.S.	**	N.S.
Prolong	Prolonged	N.S.	*	***	N.S.	***	*	N.S.	***	N.S.	N.S.	N.S.	**	N.S.
Effect of exposure system (acute *v.s.* prolonged)														
Cit	500 µg/ml	*	N.S.	**	***	***	N.S.	N.S.	N.S.	N.S.	N.S.	N.S.	***	N.S.
BSA	500 µg/ml	*	N.S.	***	N.S.	***	*	*	***	***	**	*	***	N.S.

Cit: Cit-SPIONs; BSA: BSA-SPIONs

Graphical TOC

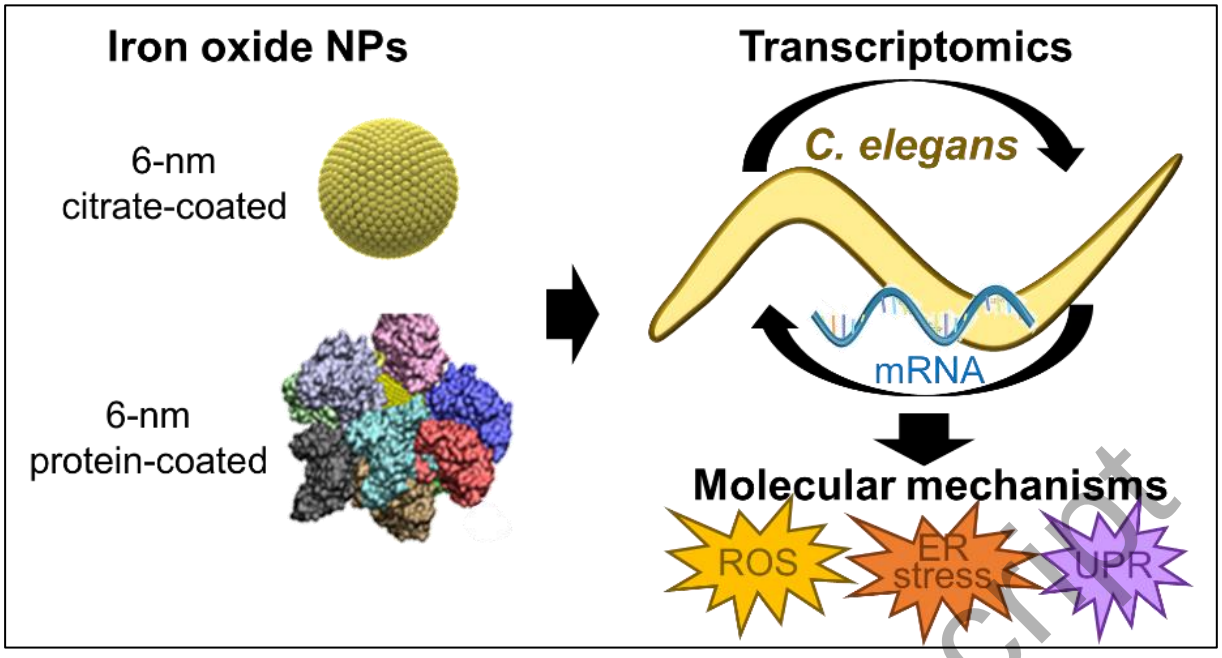

Figures

Figure 1. A) Venn diagram comparing the genes significantly affected by Cit-SPION and BSA-SPION treatment compared to untreated worms ($p<0.01$). B) Pathway enrichment analysis of genes $p<0.01$.

Figure 2. Gene expression levels, by qPCR, of very responsive genes to Cit-SPION, after treatment with Cit-SPION and BSA-SPIONs at A) 100 and B) 500 µg/ml. Three biological replicates were analyzed, and four technical repeats were used per sample. Error bars indicate the standard error of the mean. Dotted line at 1 indicates the normalized base-line expression level of control animals. T tests were used to compare treated and untreated worms and determine the *p* value. *$p<0.05$ **$p<0.01$ ***$p<0.005$.

Figure 3. Effects of SPION treatment in the selected molecular pathways, by qPCR, at A) 500 and B) 100 µg/ml. Three biological replicates were analyzed, and four technical repeats were used per sample. Error bars indicate the standard error of the mean. Dotted line at 1 indicates the normalized base-line expression level of control animals. T tests were used to compare treated and untreated worms and determine the *p* value. *$p<0.05$ **$p<0.01$ ***$p<0.005$.

Figure 4. A) Investigation of the effects of Au-NPs in the iron homeostasis genes after acute treatment by qPCR. B) Investigation of the effects of SPION treatment in the selected molecular pathways after prolonged treatment by qPCR. Three biological replicates were analyzed, and four technical repeats were used per sample. Error bars indicate the standard error of the mean. Dotted line at 1 indicates the normalized base-line expression level of control animals. T tests were used to compare treated and untreated worms and determine the *p* value. *$p<0.05$ **$p<0.01$ ***$p<0.005$.

Figure 5. A) Derivative of the mean FT-IR spectra of control (black) and SPION-treated (orange) *C. elegans*. The inset shows a zoom-in of the 1741 cm-1 band. B) Box plot of the lipid oxidation ratio (1741 cm-1/2960 cm-1) of all spectra, for control and SPION-treated animals **$p<0.01$.

Figure 6. Pathways affected by A) Cit-SPIONs (indicated in orange) and B) BSA-SPIONs (indicated in green), identified in the Pathway Enrichment Test. After Cit-SPIONs, oxidative dissolution could occur, while the BSA coating would prevent ion release from BSA-SPIONs. C) Cellular responses investigated by qPCR in SPION-treated worms.

Figure 1

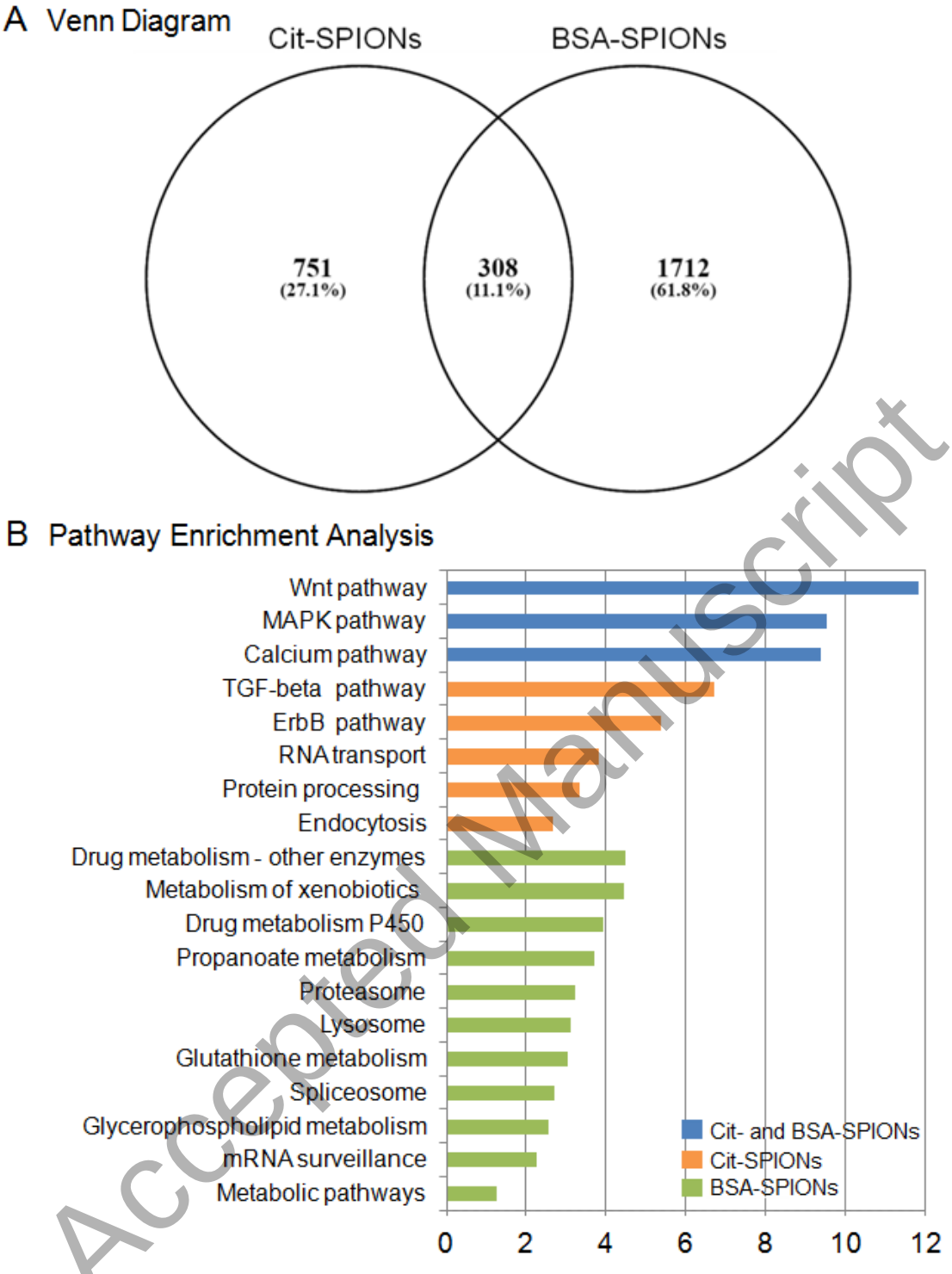

Figure 2

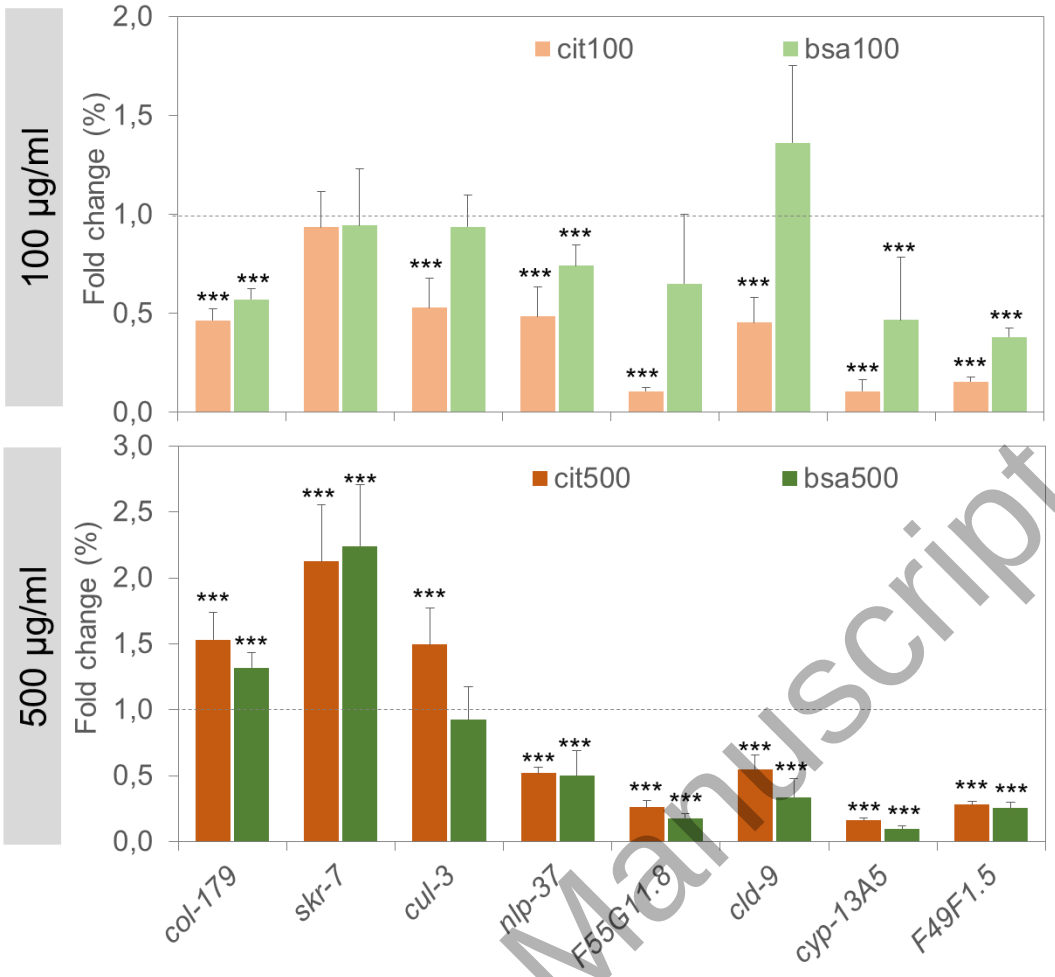

Figure 3

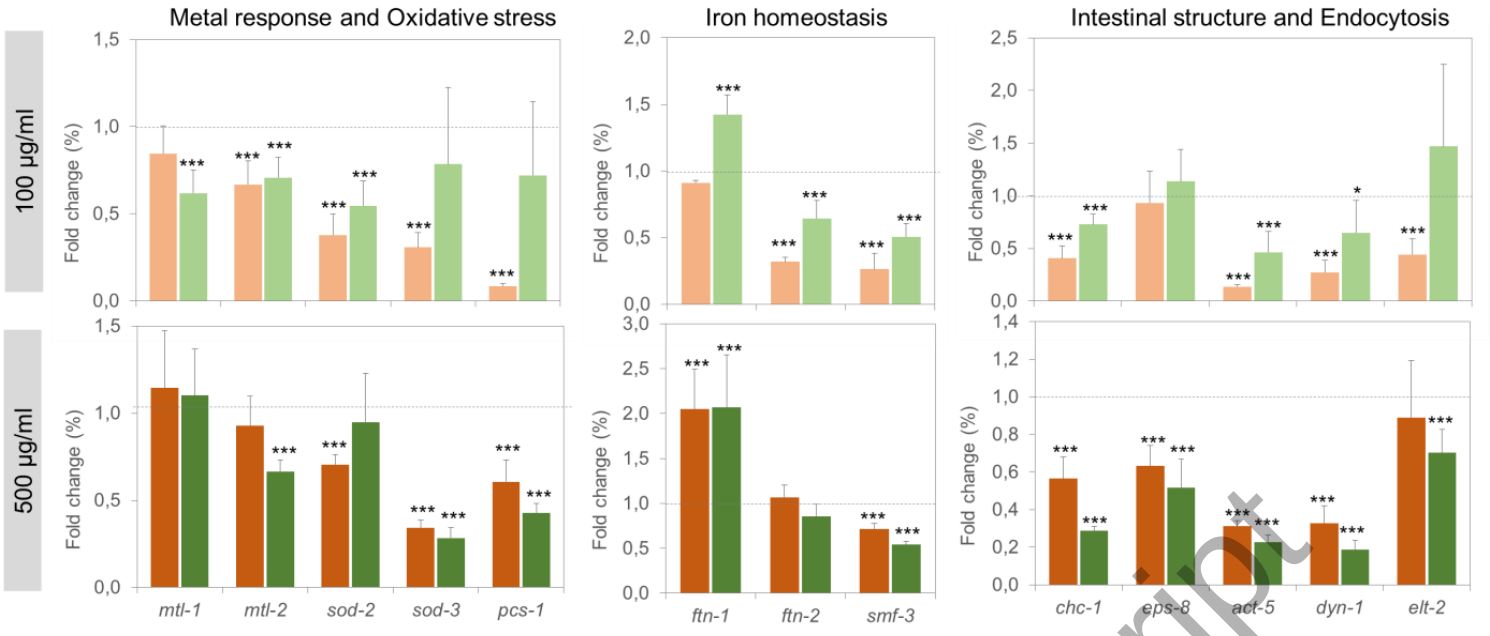

Figure 4

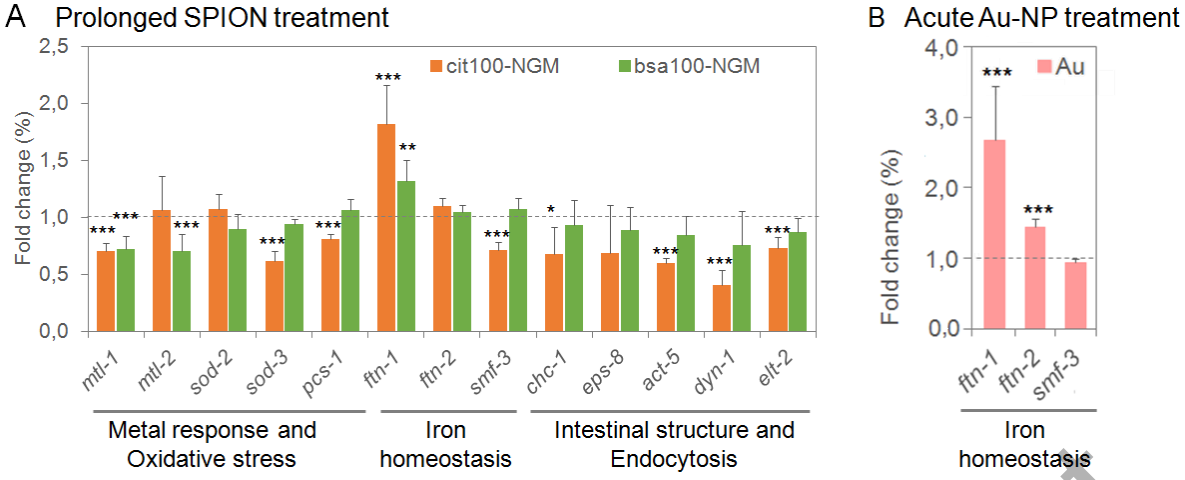

Figure 5

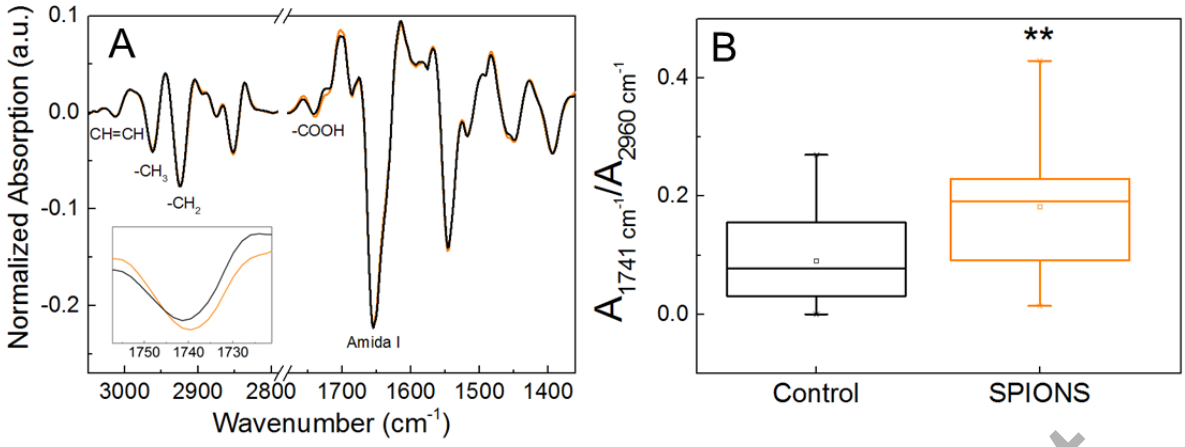

Figure 6

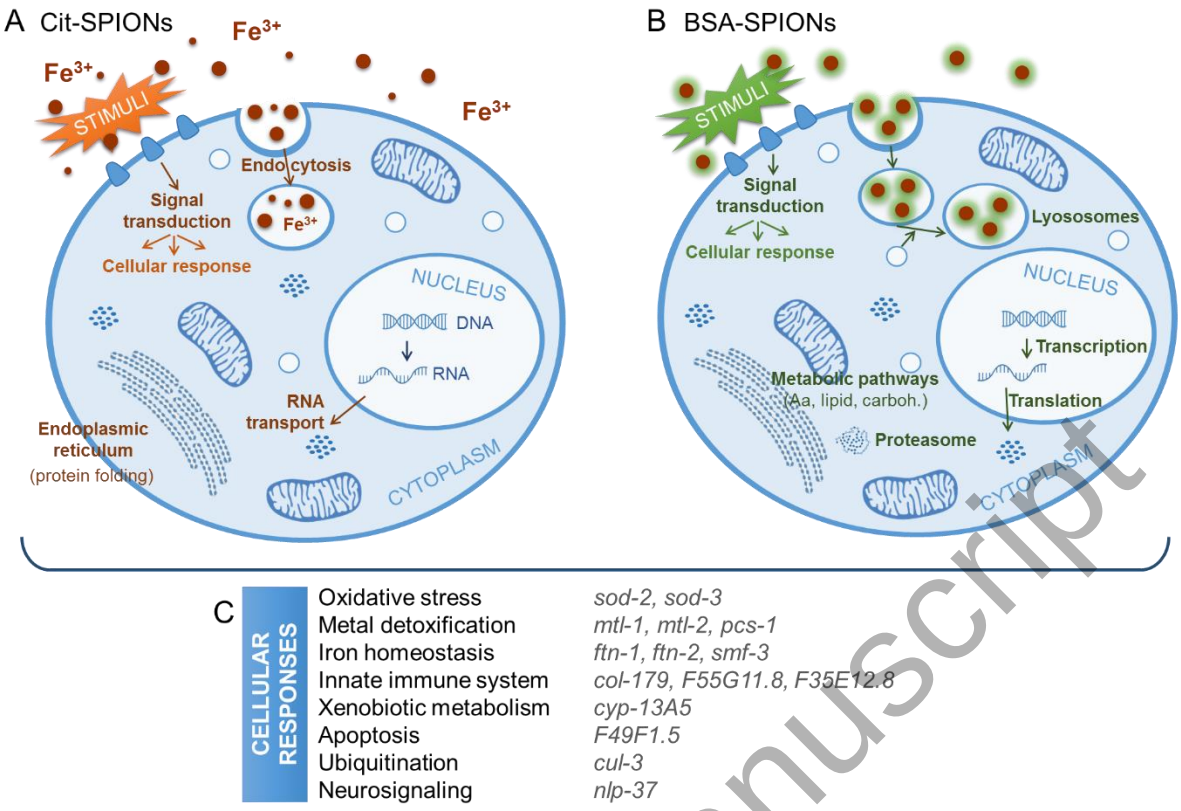

Supplementary information

Table S1. Primers and probe used in the qPCR experiments.

Gene	Forward Primer	Reverse Primer	UPL Probe	Amplicon size (bp)
act-5	CCAATCTATGAAGGATATGCCC	CATCATGTAGTCGGTCAAGTC	#158	80
chc-1	CAATGAGAGCCGATAGAACTC	TTGAGTTCACATCGAATTTCTTG	#50	144
col-179	CGAACAACTTTCTGTTACTCGTG	GCAAGTTTGTGGAGTTTGACG	#11	61
cul-3	CGAAAGAAGTTGAATCACAATAATCT	GATTGGTGACGGCATGAAG	#53	78
cyp-13A5	GGACACTTCATTATGATCCAAAAGTT	CGTCTCCAGATTCCCATCTCT	#55	78
dyn-1	GCTCCCATTGGATGGTGT	GCTGCTTGTAATCCTTGTAGATGTT	#161	116
elt-2	AGTAAACGGAGGAATGATGTG	GGTTGTCCCAAAGAAGTGCTA	#25	90
eps-8	ATATCAGAGTCGCCCATCC	GACTGTGTGAGGGTGATGGA	#131	86
F32A7.8	CCGCCTGTATCTCGTTCTCT	GGTCATGTTCGGATTGTGC	#9	71
F35E12.8	GAAGCAACATCAGGATACAATCA	TTAAATCCTGGTAGTCCAACTTGA	#19	131
F49F1.5	GATCCGAAGAATAGCGAGCA	CCGGTCGCAAAGTAGATGTT	#72	82
F55G11.8	CGAAGGATTTGCTACACTTGG	CCAACGCCATAGTTGGTATTC	#144	75
F59A6.10	GATGCAGACACCTGCATTGA	ATGGACCTGGCCTTTCATC	#95	67
ftn-1	GACGCGCACTTGACAAATTA	CATTGATCGAATGTACCTGCTC	#2	64
ftn-2	CGTGCTTCAGGACATCCA	CGGCTTCAAAAGCCTTCA	#106	68
hrp-2	CAGTGGGGTGGAAATGCT	GCATGTCGTAGCCATTGTTG	#79	67
mtl-1	CATGGCTTGCAAGTGTGACT	CACAGCAGTACTTCTCACAAC	#86	94
mtl-2	AAAAATGGTCTGCAAGTGTGA	GGCAGTTGGGCAGCAGTA	#100	111
nlp-37	ATGATGCGTTACGGCAACT	TGTAAAAACGGTATAAGACATGTGG	#11	61
pcs-1	AAGCGCCGTGGAGATTCTA	GTTGTAGATTGATTCCACTT	#159	87
R12B2.8	GACAGAAACATGTTATCCAGACACA	TCACAACATGTTCCAAATGAGA	#130	75
rla-1	ACGTCGAGTTCGAGCCATA	CCGGAAGAGACAGAAGTGATG	#162	91
scl-22	TACATACGGCCGTCGAGAA	CGTTATCAATTGGAGTACCGAAC	#87	63
skr-7	CGAGAAGGCTGCAAAGGA	GCTGCGTCCTTCTCTGTGAT	#41	63
smf-3	GCTATGGAGGGCTTTATCCA	GCCAAAGATCGGGTGATAAG	#60	68
sod-2	TTGTTCAACCGATCACAGGA	GTAAATCTGGCAGCGAGTGC	#150	60
sod-3	CACTGCTTCAAAGCTTGTTCA	ATGGGAGATCTGGGAGAGTG	#152	77
vit-1	TCAATGGAGAGAAGGAAAGCA	GGCGAACTCAGCCTTATCTC	#103	92

UPL: Universal ProbeLibrary (UPL)

Figure S1. Characterization of the tested materials: A) TEM image of Cit-SPIONs, which have a nominal size of 5.6 ± 0.8 nm. B) Negative staining TEM of BSA-SPIONs showing the inorganic core in black and the protein coating in white, with a thickness of ~3.5 nm. C) DLS measurement of Cit-SPIONs and BSA-SPIONs, revealing a ~7-nm increase in the hydrodynamic mean diameter of C-SPIONs after BSA adsorption. D) Zeta potential measurement of Cit-SPIONs and BSA-SPIONs showing less negative zeta potential for the latter attributable to the adsorption of BSA.

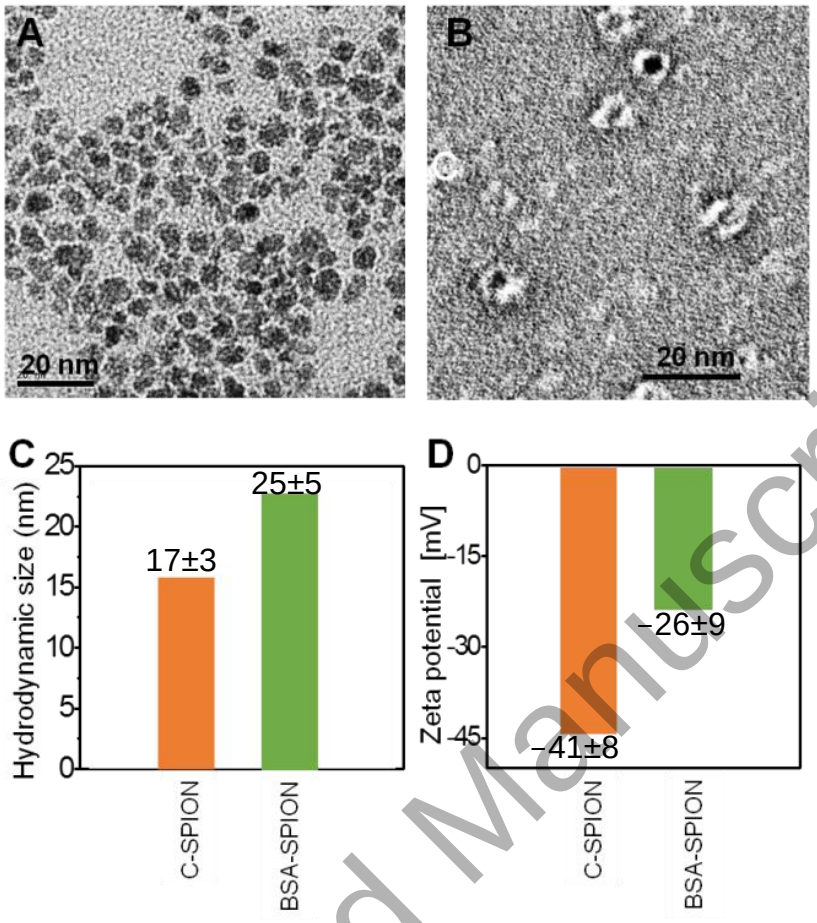

Table S2. Most up- and down-regulated genes (n=75 genes) after Cit-SPION exposure (p<0.01). Genes in bold indicate they were also studied by qPCR.

Most up-regulated		Most down-regulated	
Gene Symbol	Fold change	Gene Symbol	Fold change
nspd-4 /// nspd-5	4.56	*W06F12.7*	0.16
CELE_C17C3.15	3.74	*CELE_C27D9.2*	0.16
C30F8.5	3.50	***CELE_F59A6.10***	0.17
C30A5.4	3.35	*CELE_F41D3.11*	0.18
C48D1.10	3.28	*C54E10.11*	0.18
C10F3.12	3.22	*Y76F7A.3*	0.19
vit-1	3.19	*T25C12.5*	0.19
C40H1.12	3.02	*nlp-26*	0.19
col-179	3.01	***R12B2.8***	0.19
CELE_D2062.7	2.85	*CELE_ZC513.14*	0.20
rmd-6	2.74	*CELE_Y47H10A.5*	0.21
skr-7	2.72	*C54G7.8*	0.21
CELE_F09C6.13	2.66	***CELE_F32A7.8***	0.21
scl-22	2.64	*nlp-25*	0.22
gpr-2	2.64	*C25A6.1*	0.22
srh-284	2.64	*ZK381.44*	0.22
ora-1	2.62	*C16E9.16*	0.23
F12E12.3	2.56	*CELE_Y44A6D.2*	0.23
col-110	2.50	*cnc-2*	0.24
asns-2	2.50	*cex-1*	0.25
Y47D7A.15	2.48	***nlp-37***	0.25
ZK1053.4	2.47	*grl-4*	0.25
CELE_Y39B6A.24	2.44	*cnc-8*	0.26
rmd-4	2.34	***CELE_F55G11.8***	0.26
F01G12.12	2.34	*CELE_C25H3.10*	0.26
R02F11.6	2.33	*T24B8.12*	0.27
F25H10.9	2.31	*ZK970.7*	0.27
Y57G7A.3	2.26	*cnc-6*	0.28
M79.6	2.21	***CELE_F35E12.8***	0.28
spp-9	2.18	*K07F5.20*	0.28
ztf-11	2.16	*ZC412.13*	0.28
bli-6	2.15	*C16E9.10*	0.28
sdc-1	2.13	***cyp-13A5***	0.28
C01G8.1	2.13	*CELE_F18E3.13*	0.29
CELE_F15A8.13	2.11	*F58B4.3*	0.29
F49C5.13	2.10	*CELE_C27A7.8*	0.29
ZC250.9	2.09	***CELE_F49F1.5***	0.29
F58E6.5	2.08	*C18H9.5*	0.30
F42G9.1	2.07	*abf-2*	0.30
CELE_R09F10.8	2.06	*best-24*	0.30
meg-1	2.06	*C02B4.4*	0.30
fbxc-50	2.05	*T24F1.4*	0.31
T07D3.9	2.05	*F46C8.9*	0.31
CELE_Y75B12B.10	2.05	*CELE_R05A10.4*	0.31
CELE_F23C8.9	2.03	*ZK131.12 /// ZK131.13*	0.31
Y54F10AM.11	2.02	*ZK131.12 /// ZK131.13*	0.31
C14F11.4	2.01	*cal-4*	0.32
top-2	1.98	*F55C10.10*	0.32
rme-2	1.98	*CELE_C04E6.13*	0.32
nid-1	1.98	*H05C05.4*	0.33
fbxc-21	1.98	*B0563.9*	0.33
T22C1.9	1.98	*F41E7.14*	0.33
CELE_Y48B6A.1	1.97	*F32G8.10*	0.33
C17E7.13	1.96	*EGAP5.1*	0.33
T06D4.1	1.95	*oac-14*	0.33
ref-1	1.95	*T24B8.14*	0.34
K03A11.1	1.93	*F31F7.5*	0.34
K09E3.5	1.89	*unc-1*	0.34
CELE_C14A6.12	1.88	*K06A5.10*	0.34
glp-1	1.88	*F27D9.7*	0.34
CELE_F20D1.15	1.88	*F47C8.4*	0.34
clec-110	1.87	*F54E4.3*	0.34
fbxb-25	1.87	*F54E2.1*	0.35
C16A11.5	1.86	*T22F7.4*	0.35
T22D1.11	1.86	*CELE_M176.5*	0.35
flh-3	1.86	*str-263*	0.35
T18D3.1	1.86	*R10H10.4*	0.36
cul-3	1.84	*CELE_K03D3.2*	0.36
T13B5.9	1.84	*T01C1.4*	0.36
hrp-2	1.84	*CELE_F53F4.17*	0.36
let-418	1.83	*gpc-1*	0.37
F33H1.4	1.82	*fipr-26*	0.37
H14E04.2	1.82	*K03H9.14*	0.37
CELE_Y39F10C.3	1.81	*F02A9.1*	0.37

Table S3. Validation of the microarray experiments. The gene expression results obtained in the microarray experiments were compared to those obtained by qPCR, showing good agreement in respect of the up-/down-regulation trends (70~80% agreement overall), confirming the validity of the transcriptomic analysis.

Gene	Cit-SPIONs			BSA-SPIONs		
	Microarray	qPCR	Agreement	Microarray	qPCR	Agreement
vit-1	↑	↓	No	↑	↓	No
col-179	↑	↑	Yes	↑	↑	Yes
skr-7	↑	↑	Yes	↑	↑	Yes
F59A6.10	↓	↓	Yes	↓	↓	Yes
R12B2.8	↓	↓	Yes	↓	↓	Yes
F32A7.8	↓	↓	Yes	↓	↓	Yes
nlp-37	↓	↓	Yes	↓	↓	Yes
scl-22	↑	N.S.	No	↑	N.S.	No
cul-3	↑	↑	Yes	↑	N.S.	No
hrp-2	↑	↓	No	↑	↓	No
F55G11.8	↓	↓	Yes	↓	↓	Yes
F35E12.8	↓	↓	Yes	↓	↓	Yes
cyp-13A5	↓	↓	Yes	↓	↓	Yes
F49F1.5	↓	↓	Yes	↓	↓	Yes
%Agreement			**79%**			**71%**

↑: up-regulation; ↓: down-regulation; N.S.: Not statistically significant

Table S4. Most up- and down-regulated genes (n=75 genes) after BSA-SPION exposure (p<0.01). Genes in bold indicate they were also studied by qPCR.

Most up-regulated		Most down-regulated	
Gene Symbol	Fold change	Gene Symbol	Fold change
col-73	11.30	*CELE_C02E7.7*	0.03
E02H9.7	10.28	*col-167*	0.03
col-101	10.27	*R74.2*	0.04
col-93	9.48	*CELE_K01D12.9*	0.05
T08B2.12	9.34	*col-74*	0.05
col-135	9.08	*EGAP4.1*	0.05
nspd-7	8.18	*phat-5*	0.05
C45B2.1	8.16	*col-144*	0.05
CELE_C34D4.3	8.15	*C10F3.7*	0.05
rmd-6	7.68	*R07E5.4*	0.06
F58A6.9	6.15	*col-165*	0.06
CELE_D2062.7	5.96	*col-65*	0.07
CELE_R10E9.2	5.90	*R13H4.8*	0.07
C39B5.5	5.87	*F10D11.6*	0.07
CELE_D1086.3	5.79	*col-10*	0.07
nspd-4 /// nspd-5	5.79	*R12E2.15*	0.07
cyc-2.2	5.76	*CELE_C42D4.3*	0.07
ZK1248.4	5.75	*H10E21.4*	0.08
smy-12	5.69	*col-107*	0.08
nspd-10	5.67	*R02E4.3*	0.08
nas-20	5.47	*col-48*	0.08
Y4C6A.4	5.44	*clec-230*	0.08
CELE_F01D5.14	5.33	*CELE_B0334.13*	0.08
CELE_C12D8.24	5.27	*F45D3.15*	0.09
sdz-9	4.99	*ZC168.2*	0.09
rmd-3	4.81	*C46A5.13*	0.09
nspa-8	4.67	*ram-2*	0.09
htas-1	4.64	*B0495.15*	0.09
F58A6.9	4.60	*CELE_C08B6.17*	0.10
F58G1.12	4.54	*Y64H9A.2*	0.10
gst-29	4.52	*col-125*	0.10
CELE_F23D12.11	4.49	*ZC412.13*	0.10
vit-1	4.49	*CELE_C50F4.17*	0.10
R03G8.6	4.42	*D2096.6*	0.10
CELE_Y59E9AR.1 msp-74	4.41	*C05E7.2*	0.10
F58A6.9	4.33	*K10H10.4*	0.10
clec-223	4.22	*col-130*	0.11
ZK484.5	4.22	*R12E2.14*	0.11
C18A3.14	4.19	*CELE_T01B7.13*	0.11
CELE_Y51B9A.5	4.17	*nspb-12*	0.11
btb-11	4.11	*C06E8.5*	0.11
fbxb-43	4.06	*F53F1.4*	0.11
F09A5.1	4.06	*unc-9*	0.11
F53B6.4	4.01	*abu-14*	0.11
vet-6	3.97	*T14A8.2*	0.11
F32H2.7	3.95	*F46F3.21*	0.12
Y69E1A.1	3.93	*CELE_F32A7.8*	0.12
ttbk-2	3.93	*col-117 /// col-125 /// col-3*	0.12
CELE_Y39F10C.3	3.85	*col-117 /// col-125 /// col-3*	0.12
C54C6.7	3.84	*dod-19*	0.12
CELE_F57G9.3	3.84	*CELE_T01B7.8*	0.12
fbxc-28	3.78	*F48C1.3*	0.13
CELE_Y51H4A.5	3.77	*CELE_F59A6.10*	0.13
F11C7.6	3.76	*F35B3.4*	0.13
CELE_F09C6.13	3.75	*lips-6*	0.13
K05F6.4	3.72	*T21B6.3*	0.14
ssp-34	3.68	*pqn-71*	0.14
CELE_K08C9.2	3.64	*grl-4*	0.14
sepa-1	3.64	*CELE_F41D3.6*	0.14
CELE_F36A4.4	3.63	*C46A5.4*	0.14
thn-2	3.63	*CELE_F26G1.5*	0.14
CELE_C04G2.9	3.62	*C16D9.1*	0.15
F15E11.1 /// F15E11.14	3.61	*T24B8.14*	0.15
F15E11.1 /// F15E11.14	3.61	*CELE_F41D3.11*	0.15
acdh-8	3.61	*T21C9.9*	0.15
col-179	3.59	*K08D12.8*	0.15
Y69E1A.2	3.58	*C45B2.2*	0.15
F21F3.3	3.54	*Y47D3B.3*	0.16
EEED8.4	3.52	*F56H6.1*	0.16
T16A9.6	3.50	*pho-1*	0.16
fbxb-22	3.44	*T05B4.9*	0.16
spp-4	3.38	*phat-1*	0.16
Y71G12B.3	3.37	*CELE_F41F3.3*	0.16
CELE_F54F7.6	3.29	*phat-2*	0.16

Table S5. Common genes affected by Cit-SPIONs and BSA-SPIONs.

308 common genes affected by both Cit-SPIONs and BSA-SPIONs				
C05D10.4	*klp-18*	*nlp-19*	*rmd-1*	*F37F2.2*
F20C5.4	*unc-64*	*CELE_JC8.4*	*E02A10.4*	*rmd-6*
nlp-37	*nlp-35*	*R10H1.1*	*Y54F10AM.11*	*cutl-14*
F33D11.8	*flp-24*	*vit-1*	*F58B4.3*	*ZK757.10*
CELE_T10B9.9	*CELE_F56D5.6*	*nhr-143*	*C35E7.11*	*F10E7.9*
F39C12.4	*F56A8.3*	*W02C12.2*	*F35B12.10*	*unc-58*
CELE_F49F1.5	*cdka-1*	*CELE_T10C6.15*	*C29F3.7*	*col-172*
CELE_D1086.2	*sel-12*	*T28H10.1*	*ifb-2*	*T07F8.1*
F45E1.1	*CELE_F32A7.8*	*F27B10.1*	*unc-36*	*CELE_F48F5.6*
Y73F4A.2	*ZC443.1*	*rab-19*	*Y22D7AL.14*	*T10H9.8*
F55A4.7	*flp-18*	*nekl-2*	*C53B7.3*	*CELE_C39E9.12*
T19D7.5	*F42C5.9*	*F13H10.6*	*CELE_C27D9.2*	*CELE_D2062.7*
H23N18.6	*W03F8.6*	*C02B4.4*	*C49A1.10*	*cysl-1*
C32D5.1	*glo-3*	*CELE_C04E6.13*	*sdc-1*	*nape-2*
C35A5.6	*E02A10.3*	*str-263*	*hrg-4*	*unc-1*
tax-6	*nlp-34*	*kin-29*	*gyg-1*	*C29H12.2*
CELE_F09C6.13	*bli-6*	*F08F3.4*	*CELE_F55G11.7*	*F58D5.5*
ZK131.12 /// ZK131.13	*CELE_C03G6.17*	*aex-6*	*ZK1248.11*	*lam-2*
---	*CELE_Y69A2AR.1*	*D2045.8*	*che-2*	*alg-2*
B0228.1	*flp-7*	*pqn-36*	*exp-2*	*Y43C5A.3*
CELE_C51E3.9	*F57C9.6*	*oac-14*	*F31F7.5*	*pxl-1*
C34C6.7	*flp-6*	*lact-2*	*F14F9.8*	*F52A8.5*
C34B2.11	*F16C3.1*	*CELE_B0285.4*	*fib-1*	*dhp-1*
bath-38	*C41H7.6*	*ZK185.5*	*CELE_Y47H10A.5*	*E01A2.2*
CELE_F22D6.15	*ZK909.3*	*CELE_Y53F4B.51*	*CELE_Y75B8A.11*	*F13E6.10*
apm-1	*D1053.3*	*F47C8.4*	*ZK970.7*	*kin-1*
R07E3.1	*ZC412.13*	*CELE_C29F7.2*	*dhs-14*	*CELE_R09F10.1*
rmd-4	*K02C4.5*	*F11E6.11*	*C28G1.5*	*T19D2.3*
C38C10.6	*apc-17*	*R06C1.6*	*pes-2.1 /// pes-2.2*	*siah-1*
cnb-1	*ttr-29*	*npp-4*	*lips-10*	*nlp-1*
frm-7	*Y51F10.7*	*B0207.2*	*gpa-2*	*W10C8.4*
D2092.6	*B0507.2*	*CELE_F59A6.10*	*npp-11*	*C24A3.2*
F54A3.2	*K09H9.8*	*F21C10.3*	*pah-1*	*glt-3*
CELE_C25H3.10	*flp-26*	*T12G3.6*	*R10F2.5*	*F47B8.3*
ZK863.8	*CELE_ZC239.16*	*tag-196*	*F07C3.2*	*ptr-6*
F58B4.6	*Y54G2A.36*	*CELE_F55G11.8*	*swsn-2.2*	*tes-1*
fbxa-105	*F08G12.11*	*F38A3.3*	*rnr-2*	*ZK669.5*
act-2	*set-9*	*ins-1*	*CELE_F54D5.5*	*fbxc-21*
F56C11.5	*tnc-2*	*C28H8.11*	*hum-9*	*spt-4*
F14F11.2	*R12B2.8*	*C04E7.3*	*vhp-1*	*nhr-97*
CELE_F35E12.8	*gpc-1*	*T22D1.11*	*F58G6.9*	*CELE_ZK1307.1*
C18H9.5	*CELE_T03F6.9*	*crtc-1*	*ztf-11*	*fbxa-64*
F56C4.4	*let-526*	*nspd-4 /// nspd-5*	*T24F1.4*	*CELE_C17C3.15*
scl-22	*ttr-30*	*sulp-1*	*CELE_F33H12.7*	*ric-4*
gpb-2	*nhr-244*	*col-179*	*F42C5.4*	*E04F6.6*
abf-2	*CELE_F56H9.2*	*F43C9.7*	*glb-1*	*lin-38*
T24B8.14	*CELE_T05E12.6*	*CELE_Y44A6D.2*	*cpz-2*	*F09B9.4*
C49G7.10	*F47B8.8*	*CELE_F41D3.11*	*math-23*	*cex-1*
CELE_F46A8.7	*flp-12*	*F56F10.2*	*ags-3*	*F58E6.5*
CELE_C33A12.4	*pqn-24*	*epi-1*	*nhr-107*	*acp-2*
cri-2	*C30H6.10*	*cyb-3*	*CELE_F08D12.7*	*mig-14*
T23B12.5	*Y22D7AL.15*	*cal-1*	*R05D7.1*	*mcm-4*
C44B11.4	*CELE_M176.5*	*E04D5.5*	*atg-16.2*	*skr-17*
slo-2	*CELE_F43G6.8*	*flp-14*	*CELE_F14D7.2*	*F56H6.2*
cyp-13A5	*T25C12.5*	*mxl-3*	*CELE_F54D5.3*	*glb-19*
CELE_F17C8.3	*C39D10.7*	*F42A10.6*	*R05G6.10*	*wars-1*
hot-4	*ZK1128.7*	*flr-2*	*T08B2.15*	*K03A11.1*
CELE_T16H12.9	*grl-4*	*ptr-14*	*F08G5.3*	*F54E4.3*
zig-1	*CELE_F55D12.1*	*ZC443.3*	*CELE_W02A2.9*	*top-2*
eat-16	*D2096.9*	*his-71*	*epg-2*	*CELE_Y51A2D.14*
nhr-128	*hip-1*	*K11D12.9*	*acc-2*	
ttr-5	*F15E11.1 /// F15E11.14*	*CELE_Y39F10C.3*	*asns-2*	

Figure S2. Molecular functions and biological processes significantly affected by SPION treatment, by PANTHER bioinformatic tool. The molecular function most affected by SPION treatment was catalytic activity (~40%), followed by binding (~30%), while the most responsive biological processes were the cellular processes (~30%) followed by metabolic processes (~25%). No significant coating-dependent differences were observed in the molecular function and biological process categories.

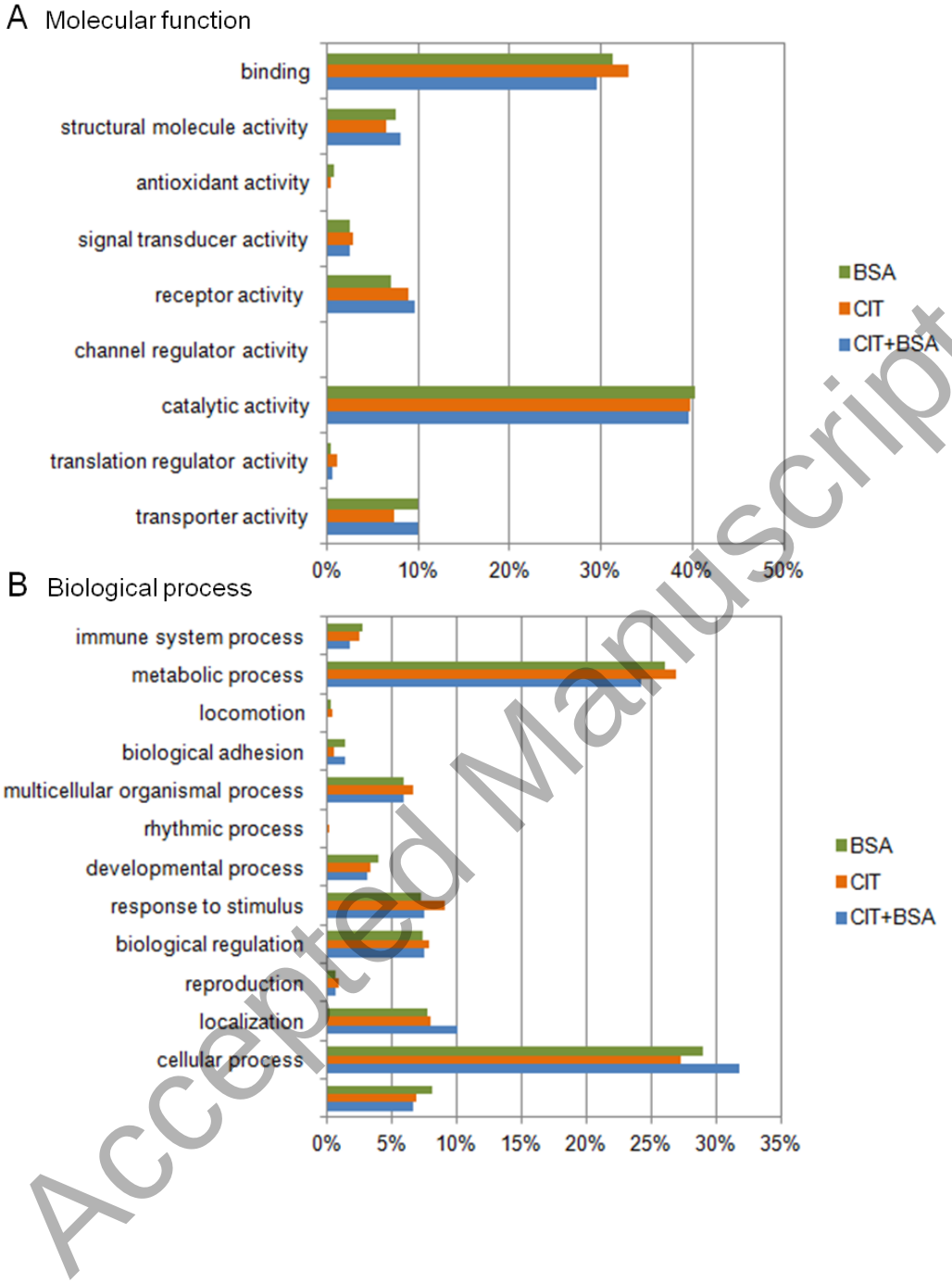

Figure S3. Effects of NP coating and exposure conditions in the selected pathways. Three biological replicates were analyzed, and four technical repeats were used per sample. Error bars indicate the standard error of the mean. Dotted line at 1 indicates the normalized base-line expression level of control animals. T tests were used to compare treated and untreated worms and determine the p value. *p<0.05 **p<0.01 ***p<0.005.

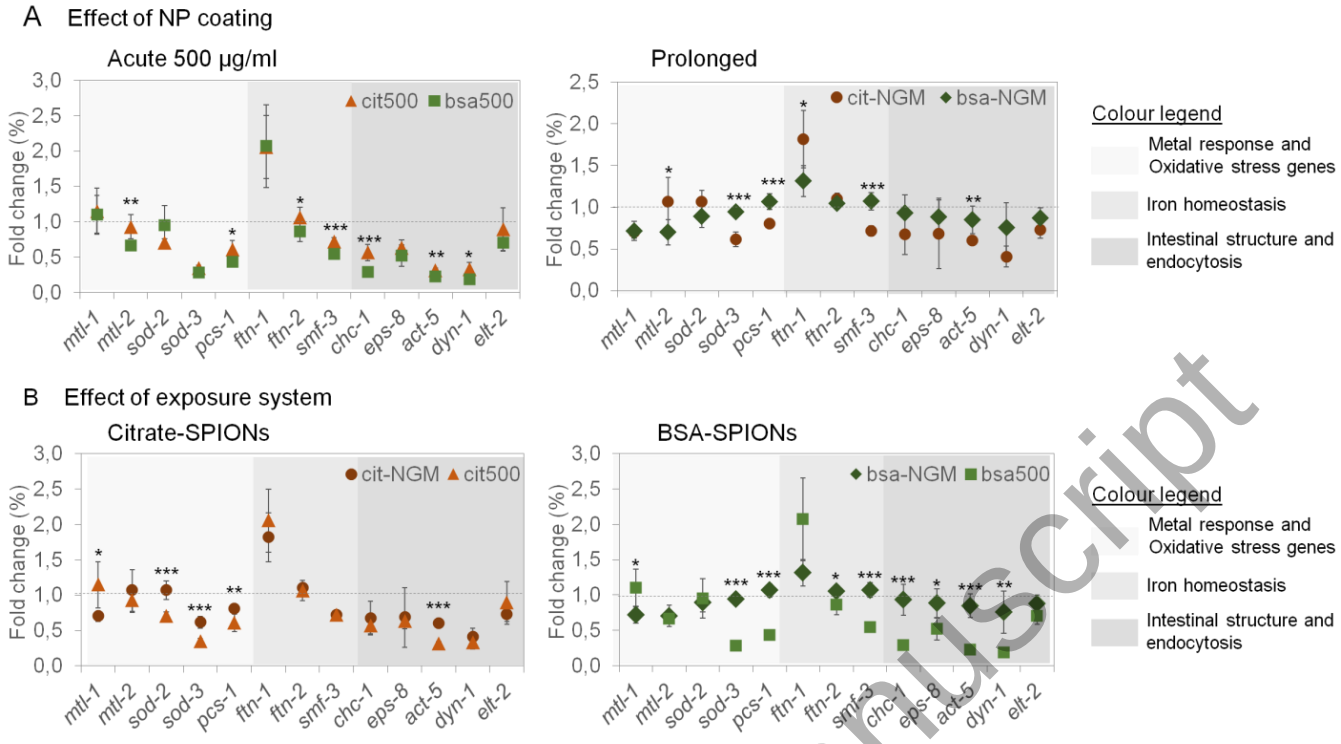

Figure S4. Effect of dose and coating in the most responsive genes to Cit-SPIONs. Three biological replicates were analyzed, and four technical repeats were used per sample. Error bars indicate the standard error of the mean. Dotted line at 1 indicates the normalized base-line expression level of control animals. T tests were used to compare treated and untreated worms and determine the p value. *p<0.05 **p<0.01 ***p<0.005.

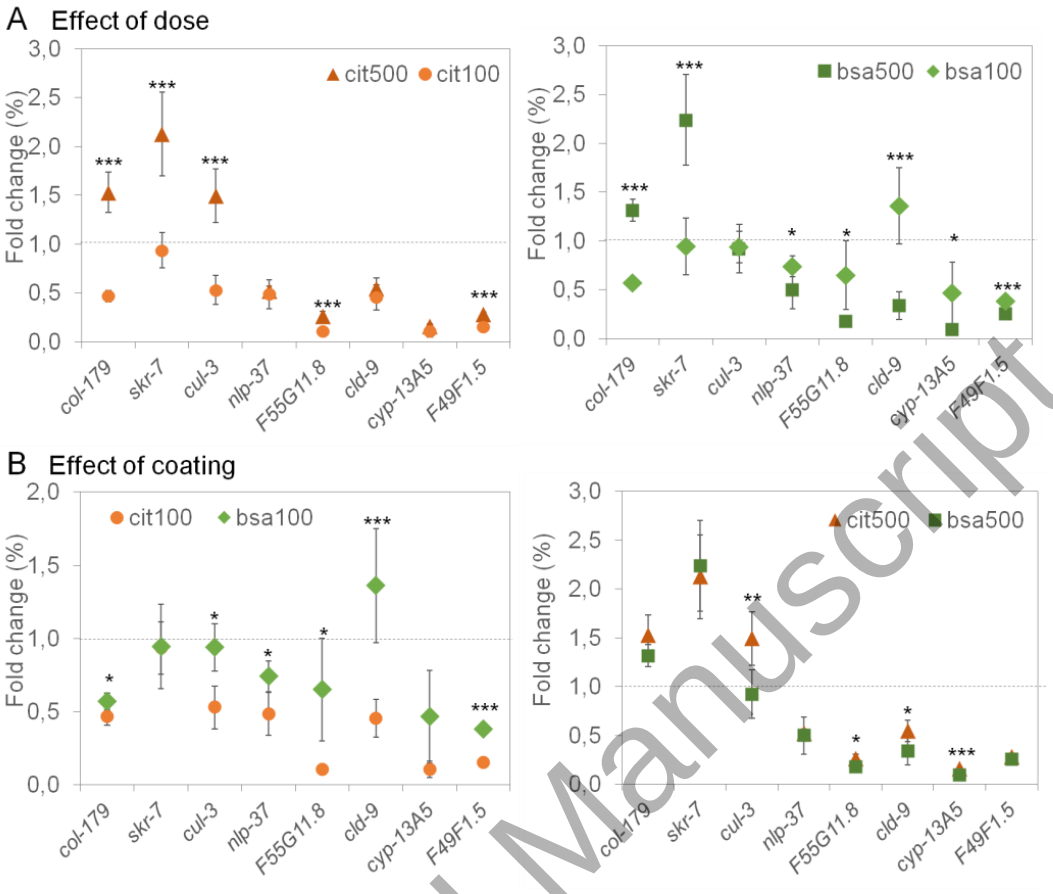

Figure S5. Characterization of the citrate-coated 11-nm gold nanoparticles by A) TEM, B) UV-Vis spectroscopy, C) DLS and D) Zeta potential. Gold nanoparticles exhibited a nominal size of 11 ± 1 nm; maximum absorption peak at 525 nm; a hydrodynamic mean diameter of 16 nm (20% polydispersity); and zeta potential of –26.4 mV.